Towards Gridless Sound Field Reconstruction

Master Thesis

I. van der Werf

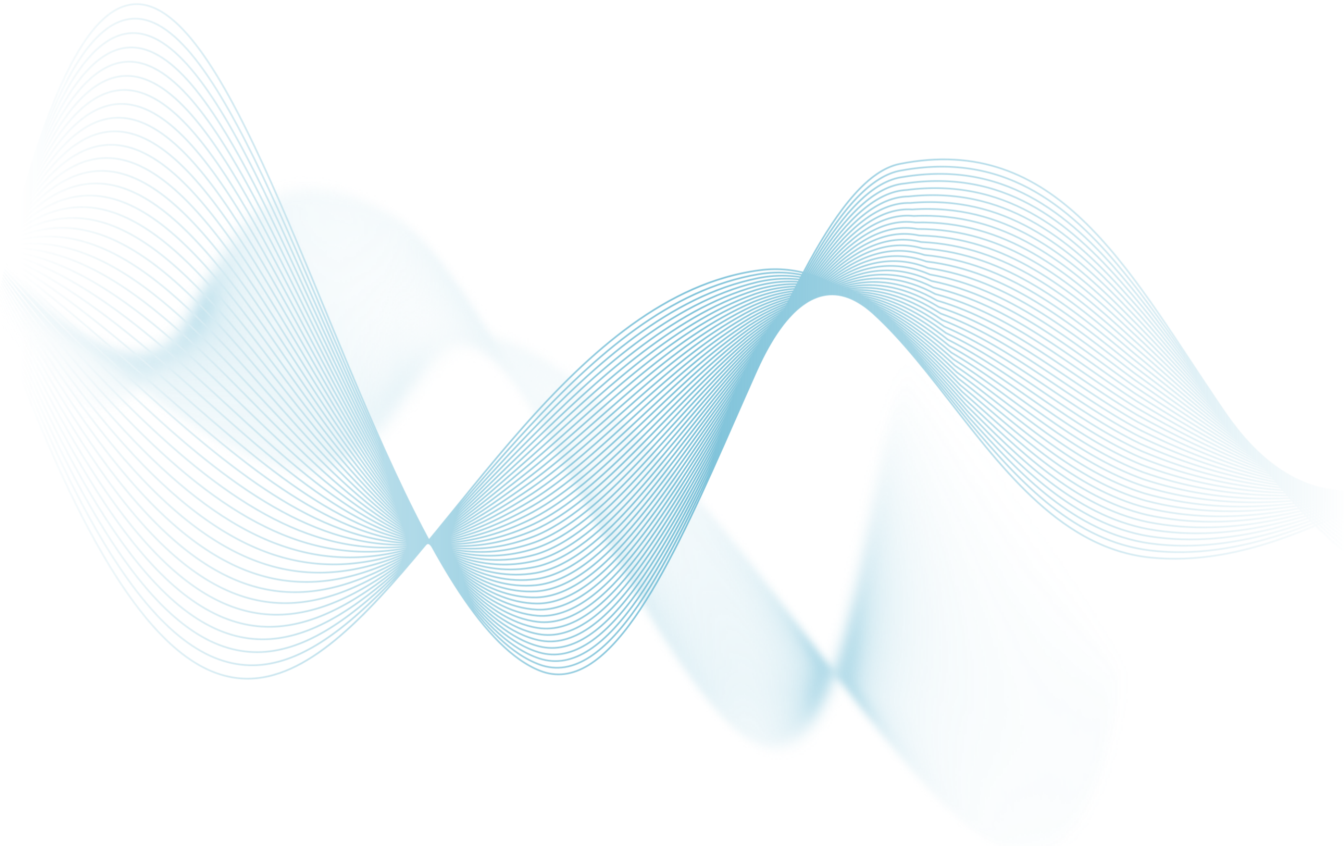

TU Delft

Towards Gridless Sound Field Reconstruction

THESIS

submitted in partial fulfillment of the
requirements for the degree of

MASTER OF SCIENCE

in

ELECTRICAL ENGINEERING

by

I. van der Werf

Bachelor of Science in Electrical Engineering,
Delft University of Technology.

Student number:	4617797	
Project duration:	September 6, 2021 - April 25, 2022	
Thesis Committee:	dr. ir. R.C. Hendriks	Chairman
	dr. M. Loog	Advisor
	dr. J. Martinez	Daily supervisor
	P. Martínez-Nuevo	(Bang & Olufsen)
	M. Møller	(Bang & Olufsen)

Delft University of Technology

Copyright © 2022 Circuits and Systems Group
All rights reserved.

"Even if there is only one possible unified theory, it is just a set of rules and equations.
What is it that breathes fire into the equations and makes a universe for them to describe?
The usual approach of science of constructing a mathematical model cannot answer
the questions of why there should be a universe for the model to describe.
Why does the universe go to all the bother of existing?"

- Stephen Hawking, A Brief History of Time

Abstract

Sound pressure varies over space and time. Knowledge about this exact behavior has many applications, e.g., room compensation, dereverberation and sound field reconstruction. Inside enclosures, the sound field is influenced by the surroundings, such as the geometry of the enclosure and the materials used. Reconstructing a satisfying sound field in the whole enclosure by extrapolating from few measurements is thus not an obvious task. The sound field in a room can be represented by a weighted sum of room modes. Thus, we can estimate the room modes and compute the sound field from it. To estimate the room modes, compressive sensing literature uses on-the-grid, sparse reconstruction methods. However, these on-the-grid methods are known to suffer from basis mismatch. In this work, we investigate the use of a gridless framework for estimating room modes using atomic norm minimization, a gridless method. The advantage of this approach is that it does not suffer from this basis mismatch problem. We derive a bound for the sound field reconstruction problem in a one-dimensional room with rigid walls and relate this to the frequency separation that is required by the atomic norm. We conclude that for perfect reconstruction of the room modes based on the investigated gridless approach, additional prior knowledge about the signal model is required. For example, knowledge about the shape of the room modes can be used. We show how recovery is possible in a one-dimensional setting by exploiting both the structure of the sound field and the acquisition method.

Preface

In September 2021 I started with my master thesis project at the Delft University of Technology, the Netherlands, that has led to the work in front of you. It was the final project for me in order to get my masters degree. I have had the privilege to collaborate on a project with the company Bang & Olufsen, located in Struer, Denmark. At both parties I had two supervisors, Jorge Martinez and Richard Hendriks from the Delft University of Technology, and Martin Møller and Pablo Martínez-Nuevo from Bang & Olufsen. Apart from two weeks in April 2022, I performed all of the work at the campus in Delft, in the research group called 'Circuits And Systems' (CAS).

After seven months of hard work I look back at a great project with lovely supervisors. I think I learned a lot about doing research, presenting results and scientific writing. Beforehand, I did not think it would be possible that I would submit a conference paper already during the project. Moreover, I'm glad that I can say that I'm a little bit proud of this work, as the final result of the master thesis project. I hope you enjoy reading it!

Finally, I think a small acknowledgment to my supervisors is in order:

Jorge, I'm very grateful for the way you have been guiding me in the process. You are always very cheerful and really find a way to spread your enthusiasm to students in general.

Richard, thank you for your great supervision. Your comments and the discussions with you often helped me to see the bigger picture.

Martin, your remarks and questions have always been sharp and on point, encouraging me to understand the problem at hand more thoroughly.

Pablo, thank you for all the time you have spend on me and my project. I absolutely loved the discussions we had, typically on some of the (more advanced) mathematics.

I. van der Werf
Struer, April 2022

Contents

Abstract v

Preface vii

Mathematical Notation xi

List of Figures xiii

List of Tables xv

1 Introduction 1
- 1.1 Motivation . . . 1
- 1.2 Introduction to Sound Field Reconstruction . . . 1
- 1.3 Prior Art . . . 2
- 1.4 Problem Statement: the basis mismatch . . . 4
- 1.5 Research Objective . . . 4
- 1.6 Outline of the Thesis . . . 4

2 Background on Sound Fields and the Atomic Norm 7
- 2.1 Sound Fields and Room Modes in 1D . . . 7
- 2.2 Atomic Norm . . . 8
  - 2.2.1 Single Measurement Vector Case . . . 8
  - 2.2.2 Multi Measurement Vector Case . . . 11
  - 2.2.3 Performance of the Atomic Norm Minimization Methods . . . 14
- 2.3 Summary . . . 15

3 Gridless framework for room mode estimation 17
- 3.1 Signal Model for a Sound Field in a 1D Room . . . 17
- 3.2 Existing On-the-grid Method . . . 18
- 3.3 Proposed Framework using the Atomic Norm . . . 19
  - 3.3.1 Bound from Modal Frequencies Separation . . . 20
  - 3.3.2 Bound from Known vs. Unknown Variables . . . 20
- 3.4 Summary . . . 21

4 Exploiting Prior Knowledge 23
- 4.1 Shape of the Steering Matrix . . . 23
- 4.2 Mirror Image Model . . . 24
- 4.3 Spectral Symmetry . . . 26
- 4.4 Summary . . . 28

5 Simulation Results 29
- 5.1 Simulation Methods . . . 29
  - 5.1.1 Dual Polynomial . . . 29
  - 5.1.2 Frequency Separation . . . 29
- 5.2 Atomic Norm without Prior Knowledge . . . 30
- 5.3 Atomic Norm with Prior Knowledge . . . 31
  - 5.3.1 Exploiting the Shape of the Steering Matrix . . . 31
  - 5.3.2 Exploiting the Mirror Image Model . . . 31
  - 5.3.3 Exploiting Spectral Symmetry . . . 33
- 5.4 Summary . . . 34

6 Conclusion **35**

7 Future Work **37**

Bibliography **39**

A EUSIPCO Paper **43**

B Derivation of the Sound Field Expression for a 1D Room with Rigid Walls **49**

C Room Modes in a Room with Non-Rigid Walls **53**

D Proof of Theorem 2.2.3 **55**

Mathematical Notation

Mathematical Notation

Throughout this work, the following notation is used.

$\mathbf{A}$	Matrix
$\mathbf{A}_i$	i'th row of a matrix
$\mathbf{a}$	Vector
a_i	i'th element of a vector
a	Scalar
$\mathbf{I}$	Identity matrix
$\mathbf{1}$	Ones matrix
$\mathbf{0}$	Zeros matrix
$\mathcal{A}$	Set
$\lvert\mathcal{A}\rvert$	Cardinality of $\mathcal{A}$
$\langle \mathbf{a}, \mathbf{b} \rangle$	Inner product of **a** and **b**
$(\cdot)^T$	Transpose
$(\cdot)^H$	Hermitian (complex conjugate transpose)
$(\cdot)^*$	Complex conjugate
$(\cdot)^\dagger$	Moore-Penrose inverse
$\mathrm{Tr}(\cdot)$	Trace operator
$\mathrm{Toep}(\cdot)$	Toeplitz operator
$\mathrm{diag}(\mathbf{A})$	Vector with diagonal elements of **A**
$\mathrm{diag}(\mathbf{a})$	Diagonal matrix with elements of **a**
$\mathrm{span}(\cdot)$	Column space
$\mathrm{conv}(\cdot)$	Convex hull
$\lvert\lvert \cdot \rvert\rvert_p$	p-norm operator
$\mathbb{R}$	Real numbers
$\mathbb{C}$	Complex numbers
$\mathbb{N}$	Natural numbers
$\mathbb{Z}$	Integer numbers
j	Imaginary unit

List of Figures

1.1 Block diagram of a sound system with feedback interacting with a sound field. The direct path is colored blue, the feedback path is colored green. 2
1.2 Living room and corresponding sound field at 150 Hz. The sets of speaker logos represent the loudspeaker arrays, the red dots represent the microphones. 3
1.3 Block diagram of the thesis outline. 5

2.1 Example of the magnitude of a dual polynomial $Q(f)$, with $M = 36$ samples and $N = 4$ frequencies. 11
2.2 The SMV case and the MMV case, simulated for $M = 20$ samples with equispaced frequencies. The probability of successful recovery is averaged over 50 Monte Carlo runs. 15

3.1 Measurement setup in a 1D room. 18
3.2 Amplitude of left and right hand side of Eq. (3.16) as a function of the room length L_x for $F = 10$, where $\frac{1}{F}$ is the distance between two consecutive microphone positions. . . . 21

4.1 Measurements including mirror image in left wall, in the case of rigid walls, $L_x = 5$. . . 25
4.2 Measurement setup in a 1D room, including the virtual measurements (in yellow) obtained from the mirror image and the added positions (dotted in gray) to form a uniform sampling grid. 26
4.3 Block diagram of the acquisition method using a moving microphone in order to remove the negative frequencies in the measured sound field. 27

5.1 Magnitude of the dual polynomial for (a) successful and (b) unsuccessful recovery. The location of the actual frequencies in the signal are indicated by vertical dotted lines. . . 30
5.2 Probability of successful recovery with respect to the frequency separation for $L = 3$ and $L = 10$ excitation frequencies, averaged over 30 Monte Carlo runs. 31
5.3 Probability of successful recovery with respect to the frequency separation, with and without constraint, averaged over 30 Monte Carlo runs. 32
5.4 Probability of successful recovery with respect to the frequency separation, with and without mirror image, averaged over 30 Monte Carlo runs. 32
5.5 Probability of successful recovery with respect to the frequency separation, with and without prior knowledge, averaged over 30 Monte Carlo runs. 33
5.6 Magnitude of dual polynomial. 34

List of Tables

5.1 Parameters used to generate Fig. 5.2. 31
5.2 Parameters used to generate Fig. 5.3. 32
5.3 Parameters used to generate Fig. 5.4. 32
5.4 Parameters used to generate Fig. 5.5. 33
5.5 Parameters used to generate Fig. 5.6. 34

1

Introduction

This chapter serves as an introduction to the master thesis. We first describe the motivation for the work in Section 1.1. Then we proceed by giving a general introduction to the problem of sound field reconstruction in Section 1.2, we give an overview of the current literature in Section 1.3 and state the problem at hand in Section 1.4. Finally the outline for the remaining part of this thesis is given in Section 1.6.

1.1. Motivation

In the past century our sensory environment has become busier then ever, people are immersed by visual and acoustic stimuli coming from all directions. Therefore the desire to partly isolate people from their surroundings has grown. This has had its repercussions on the audio industry as well, leading to applications such as noise-canceling headphones. Although the first studies can be traced back to a long time ago, currently, the behavior of sound fields and how to control them has gained renewed interest and is again an emerging research topic. Recent studies have shown that it is possible to create so-called personal sound zones; zones that can be acoustically damped with respect to each other, without a physical isolation in between them [1, 2, 3]. However, generating such sound zones is still a challenging task and is influenced by the surroundings, such as the geometry of the enclosure and the materials used. Especially in the low frequency range, the boundaries of the enclosure reflect the sound generated by the source, resulting in standing waves (later referred to as room modes). Knowledge about the shape and amplitude of these standing waves is of great importance for generating sound zones. Ideally, one would like to know the sound field at every point in space, at every point in time. In practice, this is of course not feasible as one would have to use such a large number of microphones, that they would block the physical access to the generated sound zone. This introduces a problem, as estimating the sound field from a low number of measurements is not a simple task. Current literature uses plane wave expansion as a sparse basis to represent the sound field, therefore requiring fewer microphones [4, 5, 6]. However, the reconstruction is still not perfect, and while fewer microphones are required, improvement is possible.

This is the main motivation for this master thesis, as it will focus on improving the sound field reconstruction while still using a small number of measurements, by applying new techniques to the problem. In the last decade, the atomic norm has been introduced as a continuous alternative for the sparsity promoting ℓ_1-norm [7, 8]. This work therefore investigates whether the atomic norm can be used to improve the sound field reconstruction.

1.2. Introduction to Sound Field Reconstruction

Sound is the vibration of air (or any other medium) and can be described by the air pressure changing over time. It is an acoustical wave propagating in space. Sound can be produced by a vibrating membrane, e.g. a drum or a loudspeaker.

In a living room generally multiple loudspeakers are used, for example to play music or to play the sound accompanying the video on the television. These sources together create a sound field, the air pressure as a function of time and space. To ensure high quality sound at every point in a living room or in order to create sound zones, we would like to be able to fully control the sound field. Ideally we would have a “direct” path as shown in blue in Fig. 1.1; the loudspeaker array produces sound waves which directly result in a sound field equal to the desired sound field. In practice this is unfortunately not possible as the influence of the room on the produced wound waves is not known; the reflections in a living room are highly dependent on the surroundings, e.g. the geometry of the enclosure and the materials used, and are therefore unknown beforehand.

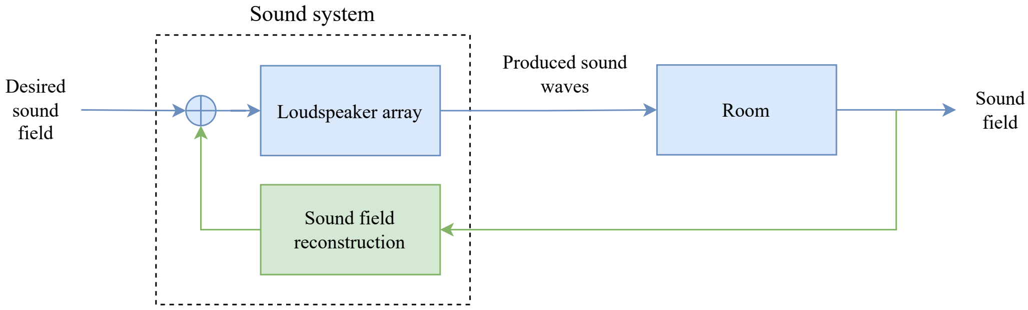

Figure 1.1: Block diagram of a sound system with feedback interacting with a sound field. The direct path is colored blue, the feedback path is colored green.

To overcome this problem, the sound system requires feedback from the room and actively adapt the sound played by the loudspeaker arrays to ensure the desired sound field is produced. This feedback loop, indicated in green in Fig. 1.1, is where sound field reconstruction comes into play. In general we measure the sound field with a set of microphones. Sound field reconstruction is the problem of reconstructing the complete sound field from these measurements.

An illustrative example of a living room (top) and its corresponding sound field (bottom) is shown in Fig. 1.2. The microphones indicated by red dots cannot be placed arbitrarily across the room, but are typically placed upon the physical objects inside the room. This means that in practice only a small number of microphones can be used. From the sound pressure measured at the microphone locations, the sound pressure in the whole room must be reconstructed, as shown in the lower half of Fig. 1.2.

In this work we will focus on the sound field reconstruction. The specific allocation of the loudspeaker arrays and the microphones is therefore out of scope of this work.

1.3. Prior Art

Knowing how the sound pressure varies over space and time has many applications, e.g., room compensation [9], dereverberation [10], and sound zone reconstruction [3]. Reconstructing sound fields inside enclosures is more difficult because the surroundings, such as the geometry of the enclosure and the materials used, influence the sound field. Reconstructing a satisfying sound field in the whole enclosure by extrapolating from few measurements is thus not an obvious task.

Several solutions for sound field reconstruction have been proposed in the past. In [11] a U-net-like neural network was implemented and trained on a large simulated data set of two dimensional boxed-shaped rooms. Although the results are promising, one can not guarantee success for new, untrained scenarios with such methods. Moreover, due to its large amount of layers, the inner working of neural networks is hard to interpret. This makes it hard to tailor a neural network to the specific problem setting or to incorporate prior knowledge about it.

Apart from deep learning methods one could also try to estimate the parameters of the assumed sound field model. With the parameters one could reconstruct the sound field. It is widely known that a sound field can be decomposed into room modes (eigenfunctions), each of them having their own modal frequencies (eigenfrequencies) (see e.g. [12, 13]). Assuming that the room modes can in its

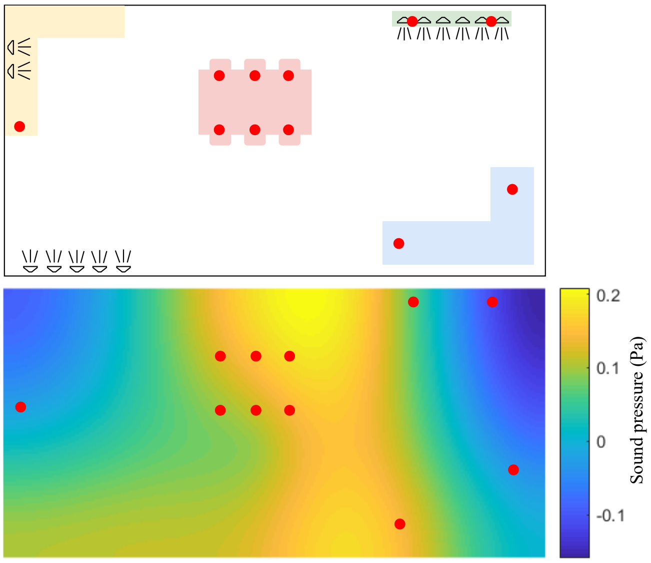

Figure 1.2: Living room and corresponding sound field at 150 Hz. The sets of speaker logos represent the loudspeaker arrays, the red dots represent the microphones.

turn be decomposed into standard (known) functions, e.g. plane waves, this means that the sound field reconstruction problem can be cast into a frequency estimation problem. Thus one has to estimate the frequencies and the corresponding weights.

Estimating (dominant) spatial frequencies has been a research topic for centuries, leading to a lot of different approaches. The methods can roughly be divided into three categories; numerical methods such as Prony's method [14], subspace based methods such as ESPRIT (see e.g. [15, 16]) and MUSIC [17] and convex optimization methods [18, 19, 20]. Numerical methods are used sporadically, e.g. [6], but often suffer from computational complexity. Subspace based methods have been very popular for estimating frequencies, however, they are not very versatile to incorporate prior knowledge about the model.

Vu *et al.* [6] consider the scenario with a non-boxed-shaped room. Assuming that the room modes (eigenfunctions) can be expanded into plane waves, two iterative approaches are proposed. These methods are based on estimating the modal parameters. Knowledge about the shape of the room modes and the modal frequencies of a room is very useful, as it allows to calculate the sound field resulting from any source-receiver pair. Thus, due to the fact that the modal parameters are estimated, the results are not bound to the measurement setup and can be used for different source receiver pairs. However, the proposed methods are a trade off between computational costs and robustness.

Last decades convex optimization methods, which are non-parametric, have proven to work quite well in general compared to the other categories (numerical and subspace based), as they have various advantages. First of all, strong theoretical guarantees can be derived even when the signal is corrupted, e.g. by noise. Second, convex optimization is very flexible to include prior knowledge and can easily be adapted to different (non-linear) measurement arrays. Lastly, in recent decades, a lot of research has been done in the field of convex optimization, presenting numerous algorithms to efficiently solve different forms of convex optimization (see e.g. [21] for a detailed overview). Therefore, state-of-the-art sound field reconstruction makes use of convex optimization methods.

In the low frequency range, the sound field can be represented by a small number of room modes [13]. Thus, another approach is to estimate room modes with compressive sensing techniques and convex optimization (see e.g. [4, 5]), due to its versatility to include prior knowledge about the setting. These approaches use methods based on the lasso problem [18], which use a sparsity promoting ℓ_1-norm. Such methods are often referred to as 'on-the-grid' methods, as they use a grid to form a basis. However, they suffer from what is called basis mismatch [22], because the assumed basis never exactly matches the actual basis of the signal. As a result on-the-grid methods will always make an approximation of the room modes, and will never produce an exact reconstruction.

1.4. Problem Statement: the basis mismatch

As discussed in the previous section, state-of-the-art sound field reconstruction suffers from basis mismatch. In this section, we will briefly discuss the basis mismatch problem. Current literature uses the ℓ_1-norm, to promote a sparse set of frequencies from a discrete grid. However, any practical grid is of finite length (computers cannot store an infinite amount of information) and thus consists of a finite amount of frequencies. Since the frequencies are real numbers, there will be infinite frequencies inside an interval, e.g. $[0, 1)$. If a frequency is chosen randomly from this interval, the chance of hitting a frequency on the grid is zero. Consequently, in practice the frequencies in a signal never lie exactly on the assumed grid. This forms a mismatch between the assumed basis $\tilde{\mathbf{A}}$ that is used for the reconstruction and the actual basis $\mathbf{A}$ of the signal. So, it is assumed that the vector $\mathbf{p}$ is a combination of a sparse set of columns of $\mathbf{A}$,

$$\mathbf{p} = \tilde{\mathbf{A}}\tilde{\mathbf{b}} \tag{1.1}$$

where b is a sparse vector, while actually,

$$\mathbf{p} = \mathbf{A}\mathbf{b}. \tag{1.2}$$

If $\mathbf{p}$ is sparse in the basis $\mathbf{A}$, then $\mathbf{b} = \mathbf{I}\mathbf{b}$ is sparse in the identity matrix, since $\mathbf{p} = \mathbf{A}\mathbf{I}\mathbf{b}$. This means that $\tilde{\mathbf{b}} = \mathbf{B}\mathbf{b}$ is actually sparse in $\mathbf{B} = \tilde{\mathbf{A}}^{-1}\mathbf{A}$, instead of in $\mathbf{I}$. Now by using the assumed basis $\tilde{\mathbf{A}}$, one assumes that $\tilde{\mathbf{A}}^{-1}\mathbf{A} = \mathbf{I}$. This inherently leads to an error, as the actual frequencies are not known beforehand, and thus there will always be a difference between the assumed and the actual basis. The larger the difference between $\mathbf{A}$ and $\tilde{\mathbf{A}}$, the larger the error of the estimation. One could make the grid of the assumed basis finer, but this will increase the size of the matrix, and thus comes with computational burden. Additionally, a finer grid will cause the frequencies to be more closely spaced and thus the columns of the basis will be more coherent, thereby worsening the reconstruction [20].

For such “on-the-grid” methods, there will be a trade-off between grid density, computational costs and coherence of the basis. This has led to new methods, which try to bypass the basis mismatch problem, and thus (ideally) also the mentioned trade-off. These new methods can be divided into two categories; “off-the-grid” and “gridless” methods. The former are methods that are more close to on-the-grid methods, as they try to match the assumed grid to the actual grid. Gridless methods tackle the problem in a completely different way, by estimating the frequencies in a continuous fashion [7, 8]. For this reason gridless methods are also known as continuous compressed sensing methods.

1.5. Research Objective

To overcome the basis mismatch problem, we investigate whether a gridless framework using the atomic norm (see e.g. [7, 8]) can be used as a replacement for the on-the-grid methods to estimate the modal frequencies. A method without basis mismatch would, in theory, improve the sound field reconstruction with respect to a method with basis mismatch. Therefore the research question is formulated as:

Is it possible to formulate a gridless framework for estimating
room modes instead of the conventional on-the-grid method? (RQ.1)

1.6. Outline of the Thesis

The remainder of this master thesis is organized as illustrated in Fig. 1.3. It is written such that the reader already familiar with room acoustics and the atomic norm minimization can sequentially read Chapter 3, in which we start the analysis of a gridless framework for room mode estimation, Chapter 4 in which we investigate how to exploit prior knowledge of the sound field, Chapter 6 in which we conclude the thesis and finally Chapter 7 in which we discuss possible future directions. Chapter 2 contains additional information about the fundamentals on which this work is based. In Chapter 5 we verify the theory that we establish in the other chapters. It is therefore an important chapter but not strictly necessary to understand our conclusion.

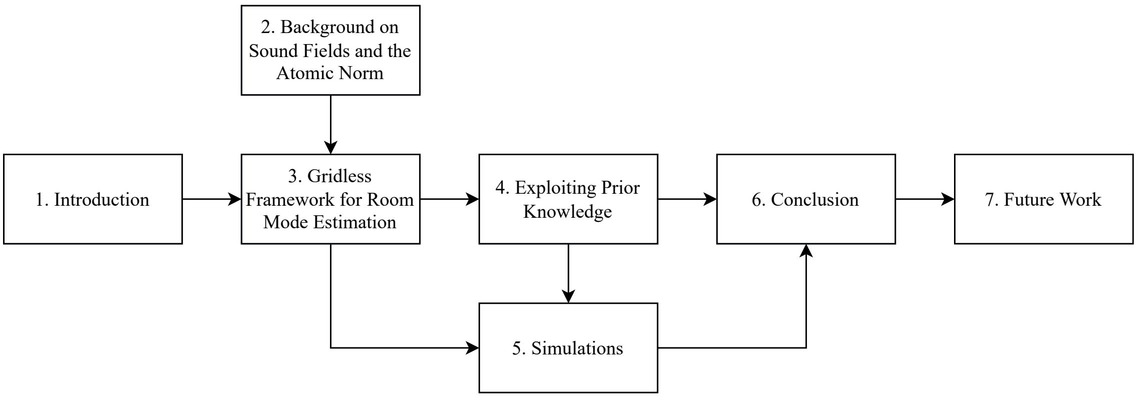
2. Background on Sound Fields and the Atomic Norm
1. Introduction
3. Gridless Framework for Room Mode Estimation
4. Exploiting Prior Knowledge
6. Conclusion
7. Future Work
5. Simulations

Figure 1.3: Block diagram of the thesis outline.

2

Background on Sound Fields and the Atomic Norm

This chapter serves as background for the methods that are applied in the other chapters. We discuss the theory that has been build by other researchers in the past.

In Section 2.1 we start this chapter with a more thorough discussion on sound fields and room modes in the one-dimensional setting. In Section 2.2 we introduce the atomic norm, both for the single and the multi measurement vector case.

2.1. Sound Fields and Room Modes in 1D

In this section, we explain what room modes are and what their shape is in a one-dimensional room with rigid walls. Moreover we discuss how the expression for the sound field in a one-dimensional room comes about.

Sound is physically represented as a change in air pressure. We can consider it as a wave that, with time, travels through space. As a consequence, a sound field should satisfy the homogeneous wave equation. We consider a wave in only one dimension. Suppose the spatial dimension is along the x-axis. We can write the wave equation in a time-independent form, which is known as the Helmholtz equation [12],

$$\frac{\partial^2 p(x,\omega)}{\partial x^2} + k^2 p(x,\omega) = 0, \quad k = \frac{\omega}{c} \tag{2.1}$$

where k is the wave number, ω and c denote the (angular) temporal frequency and the speed of wave propagation respectively, and $p(x,\omega)$ denotes the sound pressure as a function of x and ω. If we consider a sound field inside a room, we can define two boundary conditions at the walls. Suppose the case is idealized such that the room has two perfectly reflecting, rigid walls, at $x = 0$ and $x = L_x$. This introduces two boundary conditions:

$$\frac{\partial p(x,\omega)}{\partial x} = 0\Big|_{x=0,x=L_x}. \tag{2.2}$$

At the walls, the particle velocity normal to the walls is zero. Since the gradient of the sound pressure, $\frac{\partial p(x,\omega)}{\partial x}$, normal to the wall, is proportional to the particle velocity, the boundary conditions in Eq. (2.2) result. These are physically interpreted as the fact that rigid walls do not "move" with changing sound pressure and thus perfectly reflect the sound field. Solutions to Eq. (2.1) that also satisfy Eq. (2.2) constitute a discrete set and are called room modes, it can be shown (e.g. [13]) that they are given by

$$\psi_n(x) = \zeta \cos(k_n x), \quad k_n = n\frac{\pi}{L_x} \tag{2.3}$$

where ζ is a normalization factor ($\zeta = 1$ for $n = 0$ and $\zeta = \sqrt{2}$ for $n > 0$) and $n \in \mathbb{N}$. The room modes thus have distinct (spatial) frequencies, that are separated by $\frac{1}{2L_x}$. Note that the factor $e^{j\omega t}$ should be added in Eq. (2.3) to write the complete solution to the wave equation which also includes the dependency on time, instead of the time-independent solution to the Helmholtz equation.

Moreover, we can show that the room modes are mutually orthogonal (see Appendix B for the full derivation),

$$\int_0^{L_x} \psi_n(x)\psi_m(x)\mathrm{d}x = \begin{cases} L_x, & n = m \\ 0, & n \neq m. \end{cases} \tag{2.4}$$

Due to their orthogonality, the room modes can be used to form an orthogonal basis to represent the sound field in the 1D room. This implies that every sound field in the room can be shown to be a summation of weighted room modes. If a source inside the room at $x = x_0$ is emitting a single frequency $\omega = \omega_0$, the sound field is given by Eq. (2.5), that is

$$p(x,t) = -\frac{1}{L_x} e^{j\omega_0 t} \sum_{n\in\mathbb{N}} \frac{\psi_n(x_0)}{(\frac{\omega_0}{c})^2 - k_n^2} \psi_n(x). \tag{2.5}$$

In Appendix B the full derivation for the expression for the sound field with and without source is given. In Eq. (2.5) infinitely many room modes are used to represent the signal, since the summation is over all the natural numbers. In practice the signal is spatially sampled (e.g. by means of microphones) with a certain spatial sampling frequency. Due to finite sampling, the amount of room modes that can be used to uniquely reconstruct the original signal is limited. We will thus use a finite amount of room modes to represent the sound field in practice. This is justified as, assuming a bandlimited excitation, the sound field is essentially bandlimited too, thus only a finite number of room modes contribute meaningfully to the sound field.

In the lower part of the frequency spectrum, the sound field is often sparse in the spatial frequency domain as only a small amount of room modes have significant (non-zero) amplitudes [13].

If we try to retrieve the room modes, the problem can thus be cast into a sparse reconstruction problem.

2.2. Atomic Norm

In this section, we introduce the atomic norm, which can be used in convex optimization to promote a sparse solution from a continuous dictionary [7, 8]. We start with the single measurement vector (SMV) case (Section 2.2.1) and then continue with the extension towards the multi measurement vector (MMV) case (Section 2.2.2). In Section 2.2.3 we discuss the difference in performance between the SMV and the MMV case.

In this section, we will denote the signal of interest with the letter ‘y’ instead of ‘p’ since this part of the theory is not specific to our use-case of sound fields. Additionally, the assumptions on y and p will turn out to be slightly different.

2.2.1. Single Measurement Vector Case

We generally would like to decompose our signal into certain atoms. For sparse reconstruction problems this gives us the opportunity to represent the signal by a small set of atoms. Atoms can be constructed in multiple ways, but when we search for a sparse set of frequencies it makes sense to define an atom as a vector containing one frequency, $\mathbf{a}(f,\phi) \in \mathbb{C}^{|\mathcal{J}|}$ with elements $a_i(f,\phi) = e^{j(2\pi f i + \phi)}$, with $i \in \mathcal{J}$. Here $\mathcal{J}$ is the set indexing the “full uniform sampling grid”, e.g. $\mathcal{J} = \{-2K, \dots, 2K\}$, for some positive integer K.

Consequently the set of atoms is defined as

$$\mathcal{A} = \{\mathbf{a}(f,\phi) : f \in [0,1), \phi \in [0, 2\pi)\} \tag{2.6}$$

where f is the frequency of the atom, and ϕ is the phase [7]. Suppose we search for the sparsest set of atoms that can be used to represent our signal $\mathbf{y} \in \mathbb{C}^{|\mathcal{J}|}$. We can define a metric to quantify this sparsity, the so called atomic ℓ_0-norm [7], that is,

$$||\mathbf{y}||_{\mathcal{A},0} = \inf_{c_n>0, f_n\in[0,1), \phi_n\in[0,2\pi)} \Big\{|\mathcal{K}| : \mathbf{y} = \sum_{n\in\mathcal{K}} c_n \mathbf{a}(f_n,\phi_n),\ \mathbf{a}(f_n,\phi_n)\in\mathcal{A}\Big\} \tag{2.7}$$

where c_n, f_n and ϕ_n are respectively the weight, frequency and phase of the n'th atom in the signal. $\mathcal{K}$ is a set containing the indices of the atoms, thus in total the signal is composed of $|\mathcal{K}|$ atoms. However, just as the regular ℓ_0-norm, the atomic ℓ_0-norm is not convex in $\mathbf{y}$, which makes it unsuitable for convex optimization problems. We therefore turn to the atomic ℓ_1-norm [7]. Let conv() denote the convex hull, then the atomic ℓ_1-norm is defined as,

$$\begin{aligned} ||\mathbf{y}||_{\mathcal{A}} &= \inf_t\{t>0, \mathbf{y}\in t\,\mathrm{conv}(\mathcal{A})\} \\ &= \inf_{c_n>0, f_n\in[0,1), \phi_n\in[0,2\pi)} \Big\{\sum_{n\in\mathcal{K}} c_n : \mathbf{y} = \sum_{n\in\mathcal{K}} c_n \mathbf{a}(f_n,\phi_n),\ \mathbf{a}(f_n,\phi_n)\in\mathcal{A}\Big\}. \end{aligned} \tag{2.8}$$

The atomic (ℓ_1-)norm is the infimum of the sum of weights, which, multiplied with the corresponding atoms, represents the signal. So instead of measuring the number of frequencies present in the signal, the atomic norm measures the weights of these frequencies. One could look at the atomic norm as the regular ℓ_1-norm extended to the continuous domain, as the atoms of the atomic norm are continuous with respect to frequency, where the regular ℓ_1-norm is discrete. For this reason, the atomic norm is used for gridless frequency estimation.

However, the continuous frequencies do introduce some difficulties, one of them being the way to compute the value of the atomic norm; since there are infinitely many atoms in $\mathcal{A}$, this is not straight forward. Fortunately Tang *et al.* [7] established some important results. Let Tr() and Toep() be the trace and Toeplitz operator respectively. First of all, they show that for $\mathbf{y}\in\mathbb{C}^{|\mathcal{J}|}$,

$$||\mathbf{y}||_{\mathcal{A}} = \inf_{t>0, \mathbf{u}\in\mathbb{C}^{|\mathcal{J}|}} \Big\{\frac{1}{2|\mathcal{J}|}\mathrm{Tr}(\mathrm{Toep}(\mathbf{u})) + \frac{1}{2}t : \begin{bmatrix}\mathrm{Toep}(\mathbf{u}) & \mathbf{y} \\ \mathbf{y}^H & t\end{bmatrix} \succcurlyeq 0\Big\}. \tag{2.9}$$

This is a useful result, as we can thus compute the atomic norm by solving a semidefinite program. Furthermore, they presented and proved the following theorem.

Theorem 2.2.1. ([7]) *Suppose from the signal* $\mathbf{y}^\star$ *we observe the samples* $y_i^\star$,

$$y_i^\star = \sum_{n=1}^{N} b_n e^{j2\pi f_n i} \tag{2.10}$$

where $b_n\in\mathbb{C}$, *and with unknown frequencies* $\{f_1,\dots,f_N\}\subset[0,1]$ *on an index set* $\mathcal{T}\subseteq\mathcal{J}=\{-2K,\dots,2K\}$ *of size m selected uniformly at random. Thus i is a sample index, i.e.* $i\in\mathcal{T}$, *and* $|\mathcal{T}|=m$. *Additionally, assume sign*$(b_n)=b_n/|b_n|$ *are drawn i.i.d. from a symmetric distribution on the complex unit circle and*

$$\Delta_f = \min_{n_1,n_2\in\{1,\dots,N\}, n_1\neq n_2} |f_{n_1}-f_{n_2}| \tag{2.11}$$

where the distance $|f_{n_1}-f_{n_2}|$ *is understood as the wrap-around distance on the unit circle. If* $\Delta_f\geq\frac{1}{K}$, *then there exists a numerical constant C such that*

$$m \geq C\max\Big\{\log^2(\frac{K}{\delta}), N\log(\frac{N}{\delta})\log(\frac{K}{\delta})\Big\} \tag{2.12}$$

is sufficient to guarantee that with probability at least $1-\delta$, $\hat{\mathbf{y}}=\mathbf{y}^\star$ *is the unique optimizer to the following minimization problem*

$$\begin{aligned} \min_{\mathbf{y}\in\mathbb{C}^{|\mathcal{J}|}} \quad & ||\mathbf{y}||_{\mathcal{A}} \\ s.t. \quad & y_i = y_i^\star, \quad i\in\mathcal{T} \end{aligned} \tag{2.13}$$

or equivalently

$$
\begin{aligned}
\min_{t>0,\mathbf{u}\in\mathbb{C}^{|\mathcal{J}|},\mathbf{y}\in\mathbb{C}^{|\mathcal{J}|}} \quad & \frac{1}{2|\mathcal{J}|}\mathrm{Tr}(\mathrm{Toep}(\mathbf{u})) + \frac{1}{2}t \\
s.t. \quad & \begin{bmatrix} \mathrm{Toep}(\mathbf{u}) & \mathbf{y} \\ \mathbf{y}^H & t \end{bmatrix} \succcurlyeq 0 \\
& y_i = y_i^\star, \quad i \in \mathcal{T}.
\end{aligned}
\tag{2.14}
$$

This theorem states that if the frequencies are separated well enough with respect to the number of measurements ($\Delta_f \geq \frac{1}{K}$), the optimal value $\mathbf{y} = \hat{\mathbf{y}}$ in the semi-definite program (SDP) will be exactly equal to the original signal $\mathbf{y}^\star$. For example, we can measure the signal at $M = |J| = 4K+1$ points, and reconstruct the signal (perfectly) by minimizing the atomic norm, proviso the frequencies are separated by $\Delta_f \geq \frac{\alpha}{M-1}$, for $\alpha = 4$. This bound was later improved by C. Fernandez-Granda [23] to $\alpha = 2.52$, where it is also reasoned that the bound can inherently not be lower than $\alpha = 2$. However, (although not proven) in practice the bound seems to be lower; in Section 2.2.3 we will look at its value in practice.

Note that the solution to the SDP does not directly provide the desired frequencies, hence, we will discuss how to extract the frequencies.

Frequency retrieval via the dual polynomial

A remarkable fact is that the atomic norm allows us to estimate the frequencies in the original signal with infinite precision. The frequencies can be retrieved by using the dual solution of $\hat{\mathbf{y}}$. The dual problem of Eq. (2.13) is given by (see [7, 21]),

$$
\begin{aligned}
\max_{\mathbf{q}\in\mathbb{C}^{|\mathcal{J}|}} \quad & \langle \mathbf{q}_{\mathcal{T}}, \mathbf{y}^\star_{\mathcal{T}} \rangle_{\mathbb{R}} \\
\text{s.t.} \quad & ||\mathbf{q}||^*_{\mathcal{A}} \leq 1 \\
& q_i = 0, \quad i \notin \mathcal{T}.
\end{aligned}
\tag{2.15}
$$

Here the dual norm $||\cdot||^*_{\mathcal{A}}$ of the atomic norm $||\cdot||_{\mathcal{A}}$ is defined as

$$
||\mathbf{q}||^*_{\mathcal{A}} = \sup_{||y||_{\mathcal{A}}\leq 1} \langle \mathbf{q}, \mathbf{y} \rangle_{\mathbb{R}} = \sup_{f\in[0,1),\phi\in[0,2\pi)} \langle \mathbf{q}, e^{j\phi}\mathbf{a}(f,0) \rangle_{\mathbb{R}} = \sup_{f\in[0,1)} \langle \mathbf{q}, \mathbf{a}(f,0) \rangle_{\mathbb{R}}. \tag{2.16}
$$

Now if there exist a dual polynomial,

$$
Q(f) = \langle \mathbf{q}, \mathbf{a}(f,0) \rangle = \sum_{i\in\mathcal{J}} q_i e^{-j2\pi i f} \tag{2.17}
$$

satisfying the conditions

$$
\begin{aligned}
Q(f) &= \mathrm{sign}(c_n), \quad \forall f \in \{f_1, \ldots, f_N\} \\
|Q(f)| &< 1, \quad \forall f \notin \{f_1, \ldots, f_N\} \\
q_i &= 0, \quad \forall i \notin \mathcal{T}
\end{aligned}
\tag{2.18}
$$

then $\hat{\mathbf{y}} = \mathbf{y}^\star$ is the unique optimizer to Eq. (2.13) [7].

Tang *et al.* [7] show that, under the conditions of Theorem 2.2.1, one is able to construct such a dual polynomial, thereby proving that $\mathbf{y} = \mathbf{y}^\star$ is the unique optimizer of the atomic norm minimization problem. The existence of the dual polynomial is thus used to prove Theorem 2.2.1. Additionally, the dual polynomial is useful for retrieving frequencies. By using the dual solution $\mathbf{q}$, we can construct the dual polynomial $Q(f)$, which will attain the value one if and only if $f \in \{f_1, \ldots, f_N\}$. Since $Q(f)$ is a function of the frequency, we can retrieve the frequencies of the signal with infinite precision. An example of a dual polynomial for a signal with four frequencies is shown in Fig. 2.1.

Frequency retrieval via the Toeplitz matrix

Apart from the dual polynomial, the frequencies can also be estimated from the Toeplitz matrix $\mathrm{Toep}(\hat{\mathbf{u}})$.

First note that all the observed samples $y_i^\star$ are stacked in a vector to form $\mathbf{y}^\star$. This vector can be written as,

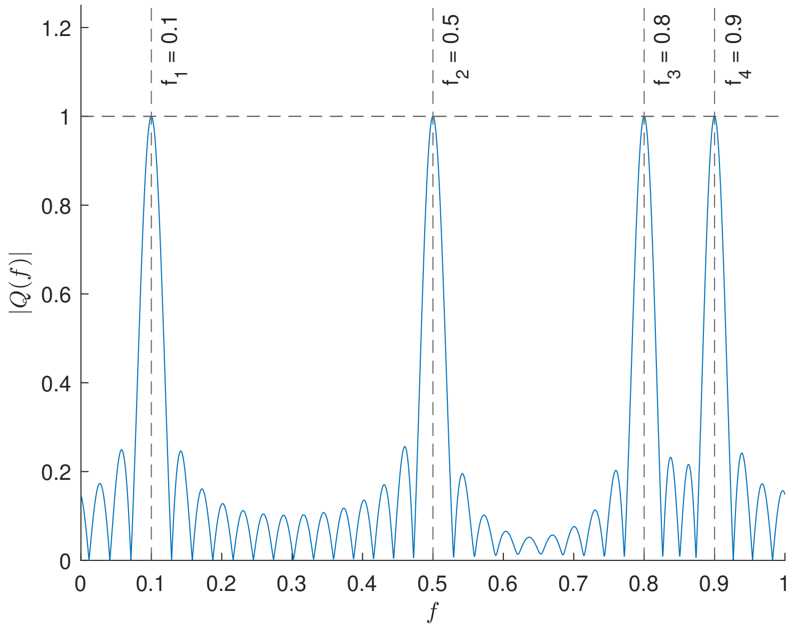

Figure 2.1: Example of the magnitude of a dual polynomial $Q(f)$, with $M = 36$ samples and $N = 4$ frequencies.

$$\begin{aligned}\mathbf{y}^\star &= \sum_{n=1}^{N} c_n \mathbf{a}(f_n, \phi_n), \quad c_n > 0, \mathbf{a}(f_n, \phi_n) \in \mathcal{A} \\ &= \sum_{n=1}^{N} c_n \mathbf{a}(f_n) e^{j\phi_n} \\ &= \mathbf{A}\mathbf{s}\end{aligned} \tag{2.19}$$

where the vector $\mathbf{a}(f_n) \in \mathbb{C}^M$ has elements $a_i(f_n) = e^{j2\pi f_n i}$, $\mathbf{A} = [\mathbf{a}(f_1), \dots, \mathbf{a}(f_N)] \in \mathbb{C}^{M \times N}$ and $\mathbf{s} = [c_1 e^{j\phi_1}, \dots, c_N e^{j\phi_N}]^T$.

If we now look at the positive semidefinite matrix with the optimal parameters, $\hat{\mathbf{u}}$, $\hat{t}$, and (assuming we meet the frequency separation $\Delta_f \geq \frac{1}{K}$) $\hat{\mathbf{y}} = \mathbf{y}^\star$, then the positive semidefinite matrix can be decomposed as,

$$\begin{bmatrix} \text{Toep}(\hat{\mathbf{u}}) & \mathbf{y}^\star \\ \mathbf{y}^{\star H} & \hat{t} \end{bmatrix} = \begin{bmatrix} \mathbf{AZA}^H & \mathbf{As} \\ \mathbf{s}^H \mathbf{A}^H & \sum_n^N c_n \end{bmatrix} = \sum_n^N c_n \begin{bmatrix} \mathbf{a}(f_n) \\ 1 \end{bmatrix} \begin{bmatrix} \mathbf{a}(f_n) \\ 1 \end{bmatrix}^H \succcurlyeq 0 \tag{2.20}$$

where $\mathbf{Z} = \text{diag}(\{c_1, \dots, c_N\})$. The optimal Toeplitz matrix is therefore, $\hat{\mathbf{T}} = \text{Toep}(\hat{\mathbf{u}}) = \mathbf{AZA}^H$. Thus, we first solve the SDP in Eq. (2.14) and from the optimal Toeplitz matrix the frequencies can be retrieved by means of subspace methods such as ESPRIT [15]. In practice the frequencies will be retrieved via the optimal Toeplitz matrix, and not via the dual polynomial. The reason being that the dual polynomial is sensitive to noise, and the fact that the calculation via the dual polynomial takes more time, because the function $Q(f)$ must be evaluated at a lot of points to get an acceptable resolution. However, the dual polynomial does play an important role in the proof of Theorem 2.2.1, and can therefore often be used for illustrative purposes.

2.2.2. Multi Measurement Vector Case

Until now we have considered the SMV case, where the data is represented in a single vector. However, for the application to sound fields we might benefit from a MMV setup, since it allows to sample in one more dimension, e.g. sampling in both space and time. The MMV case will allow for more measurements and can thus incorporate more information. This gives reason to investigate the atomic norm for the MMV case.

In the SMV case we considered a vector $\mathbf{y} \in \mathbb{C}^{|\mathcal{J}|}$, which was sparse in the (spatial) frequency domain. Similarly, in the MMV case we have a matrix $\mathbf{Y} \in \mathbb{C}^{|\mathcal{J}| \times L}$, of which the columns are jointly sparse.

Let's first redefine the atomic set to a more general definition. We write

$$\mathcal{A} = \{\mathbf{a}(f, \boldsymbol{\phi}) = \mathbf{a}(f)\boldsymbol{\phi} \; : f \in [0,1), \boldsymbol{\phi} \in \mathbb{C}^{1\times L}, ||\boldsymbol{\phi}||_2 = 1\} \tag{2.21}$$

where $\mathbf{a}(f) \in \mathbb{C}^{|\mathcal{J}|}$ with elements $a_i(f) = e^{j2\pi f i}$, $i \in \mathcal{J}$. If $L = 1$, this atomic set coincides with the SMV case, given by Eq. (2.6). Then, the atomic ℓ_0-norm in the MMV case becomes

$$||\mathbf{Y}||_{\mathcal{A},0} = \inf_{c_n>0, f_n\in[0,1), \boldsymbol{\phi}_n \in \mathbb{C}^{1\times L}} \Big\{|\mathcal{K}| : \mathbf{Y} = \sum_{n\in\mathcal{K}} c_n \mathbf{a}(f_n, \boldsymbol{\phi}_n), \; a(f_n, \boldsymbol{\phi}_n) \in \mathcal{A}\Big\}. \tag{2.22}$$

Similarly the atomic (ℓ_1-)norm is defined as

$$\begin{aligned} ||\mathbf{Y}||_{\mathcal{A}} &= \inf_t \{t > 0, \mathbf{Y} \in t\mathrm{conv}(\mathcal{A})\} \\ &= \inf_{c_n>0, f_n\in[0,1), \boldsymbol{\phi}_n \in \mathbb{C}^{1\times L}} \Big\{\sum_{n\in\mathcal{K}} c_n : \mathbf{Y} = \sum_{n\in\mathcal{K}} c_n \mathbf{a}(f_n, \boldsymbol{\phi}_n), \; \mathbf{a}(f_n, \boldsymbol{\phi}_n) \in \mathcal{A}\Big\}. \end{aligned} \tag{2.23}$$

Yang *et al.* [24] showed that the atomic norm $||\mathbf{Y}||_{\mathcal{A}}$, where $\mathbf{Y} \in \mathbb{C}^{M\times L}$, can be computed with the following SDP

$$\begin{aligned} \min_{\mathbf{W}\in\mathbb{C}^{L\times L}, \mathbf{u}\in\mathbb{C}^{M}} \quad & \frac{1}{2\sqrt{M}}\left[\mathrm{Tr}(\mathrm{Toep}(\mathbf{u})) + \mathrm{Tr}(\mathbf{W})\right] \\ \text{s.t.} \quad & \begin{bmatrix} \mathbf{W} & \mathbf{Y}^H \\ \mathbf{Y} & \mathrm{Toep}(\mathbf{u}) \end{bmatrix} \succcurlyeq 0. \end{aligned} \tag{2.24}$$

Moreover, the following theorem is presented and proved.

Theorem 2.2.2. (Theorem 5 in [24]) *Suppose we observe*

$$\mathbf{Y}^\star = \sum_{n=1}^{N} c_n \mathbf{a}(f_n, \boldsymbol{\phi}_n) \tag{2.25}$$

where $c_n > 0$, and with unknown frequencies $\{f_1, ..., f_N\} \subset [0,1]$ on the index set $\mathcal{T} \times \{1, ..., L\}$, where $\mathcal{T} \subseteq \mathcal{J} = \{-2K, \dots, 2K\}$ is of size m and selected uniformly at random. Assume that $\{\boldsymbol{\phi}_n\}_{n=1}^N \in \mathbb{C}^{1\times L}$ such that $||\boldsymbol{\phi}_n|| = 1$ are independent random variables with $\mathbb{E}[\boldsymbol{\phi}_n] = \mathbf{0}$. Let $M = |\mathcal{J}|$. If $\Delta_f = \frac{1}{\lfloor (K-1)/4 \rfloor}$, then there exists a numerical constant C such that

$$m \geq C \max\Big\{\log^2(\frac{\sqrt{L}M}{\delta}), N\log(\frac{N}{\delta})\log(\frac{\sqrt{L}M}{\delta})\Big\} \tag{2.26}$$

is sufficient to guarantee that, with probability at least $1-\delta$, $\hat{\mathbf{Y}} = \mathbf{Y}^\star$ is the unique optimizer to

$$\begin{aligned} \min_{\mathbf{Y}\in\mathbb{C}^{|\mathcal{J}|\times L}} \quad & ||\mathbf{Y}||_{\mathcal{A}} \\ \text{s.t.} \quad & \mathbf{Y}_i = \mathbf{Y}_i^\star, \quad i \in \mathcal{T} \end{aligned} \tag{2.27}$$

or equivalently,

$$\begin{aligned} \min_{\mathbf{W}\in\mathbb{C}^{L\times L}, \mathbf{u}\in\mathbb{C}^{|\mathcal{J}|}, \mathbf{Y}\in\mathbb{C}^{|\mathcal{J}|\times L}} \quad & \mathrm{Tr}(\mathrm{Toep}(\mathbf{u})) + \mathrm{Tr}(\mathbf{W}) \\ \text{s.t.} \quad & \begin{bmatrix} \mathbf{W} & \mathbf{Y}^H \\ \mathbf{Y} & \mathrm{Toep}(\mathbf{u}) \end{bmatrix} \succcurlyeq 0 \\ & \mathbf{Y}_i = \mathbf{Y}_i^\star, \quad i \in \mathcal{T} \end{aligned} \tag{2.28}$$

and $\mathbf{Y}^\star = \sum_{n=1}^N c_n \mathbf{a}(f_n, \boldsymbol{\phi}_n)$ is the unique atomic decomposition satisfying that $||\mathbf{Y}^\star||_{\mathcal{A}} = \sum_{n=1}^N c_n$.

Thus we have a similar result for the MMV case; if we consider the ‘full data’ case, we measure the signal at $M = |J| = 4K + 1$ points, we can reconstruct the signal by minimizing the atomic norm, provided that the frequencies are separated by $\Delta_f \geq \frac{\alpha}{M-1}$, for $\alpha = 4$. This bound holds for all MMV cases, thus also for the ’worst case’ in which the vectors are dependent. This is one of the reasons why the bound is not relaxed compared to the SMV case. However, also for the case with independent columns it has not been proven yet that this bound can be improved. However, in practice we do see improvement, as we will show later on in Section 2.2.3.

Using Theorem 2.2.3, the matrix in Eq. (2.28) can be rewritten. The proof of the theorem is a contribution of this thesis and is given in Appendix D.

Theorem 2.2.3. *Suppose* $\mathbf{U} = \begin{bmatrix} \mathbf{A} & \mathbf{B}^H \\ \boldsymbol{B} & \boldsymbol{C} \end{bmatrix} \in \mathbb{C}^{N \times N}$. *Then,* $\boldsymbol{U} \succcurlyeq 0$ *if and only if* $\begin{bmatrix} \boldsymbol{C} & \boldsymbol{B} \\ \boldsymbol{B}^H & \boldsymbol{A} \end{bmatrix} \succcurlyeq 0$.

This way, the matrix in the SDP for the MMV case has a similar structure as in the SMV case. Only columns and rows are added on the right and bottom respectively, corresponding to the extra measurement vectors,

$$\begin{aligned} \min_{\mathbf{W} \in \mathbb{C}^{L \times L}, \mathbf{u} \in \mathbb{C}^{|\mathcal{J}|}, \mathbf{Y} \in \mathbb{C}^{|\mathcal{J}| \times L}} \quad & \operatorname{Tr}(\operatorname{Toep}(\mathbf{u})) + \operatorname{Tr}(\mathbf{W}) \\ \text{s.t.} \quad & \begin{bmatrix} \operatorname{Toep}(\mathbf{u}) & \mathbf{Y} \\ \mathbf{Y}^H & \mathbf{W} \end{bmatrix} \succcurlyeq 0 \\ & \qquad\qquad \mathbf{Y}_i = \mathbf{Y}_i^\star, \quad i \in \mathcal{T}. \end{aligned} \tag{2.29}$$

Again, the frequencies can be retrieved with infinite precision, using the solution to the dual problem. The dual problem of Eq. (2.27) is given by

$$\begin{aligned} \max_{\mathbf{V} \in \mathbb{C}^{|\mathcal{J}| \times L}} \quad & \langle \mathbf{V}_\mathcal{T}, \mathbf{Y}_\mathcal{T}^\star \rangle_\mathbb{R} \\ \text{s.t.} \quad & ||\mathbf{V}||_\mathcal{A}^* \leq 1 \\ & \quad \mathbf{V}_i = 0, \quad i \notin \mathcal{T}. \end{aligned} \tag{2.30}$$

Here the dual norm of $|| \cdot ||_\mathcal{A}$ is defined as

$$\begin{aligned} ||\mathbf{V}||_\mathcal{A}^* &= \sup_{||\mathbf{Y}||_\mathcal{A} \leq 1} \langle \mathbf{V}, \mathbf{Y} \rangle_\mathbb{R} = \sup_{\mathbf{a}(f, \boldsymbol{\phi}) \in \mathcal{A}} \langle \mathbf{V}, \mathbf{a}(f, \boldsymbol{\phi}) \rangle_\mathbb{R} \\ &= \sup_{f \in [0,1), \boldsymbol{\phi} \in \mathbb{C}^{1 \times L}, ||\boldsymbol{\phi}||_2 = 1} \langle \mathbf{a}(f)^H \mathbf{V}, \boldsymbol{\phi} \rangle_\mathbb{R} = \sup_{f \in [0,1)} ||\mathbf{a}(f)^H \mathbf{V}||_2 \end{aligned} \tag{2.31}$$

Where $\langle \mathbf{A}, \mathbf{B} \rangle_\mathbb{R} = \operatorname{Re}\{\operatorname{Tr}(\mathbf{B}^H \mathbf{A})\}$.

Similar to the SMV case, if there exist a dual polynomial,

$$Q(f) = \mathbf{a}(f)^H \mathbf{V} \tag{2.32}$$

satisfying the conditions

$$\begin{aligned} Q(f) &= \boldsymbol{\phi}_n, \quad \forall f \in \{f_1, \ldots, f_N\} \\ ||Q(f)||_2 &< 1, \quad \forall f \notin \{f_1, \ldots, f_N\} \\ \mathbf{V}_i &= 0, \quad \forall i \notin \mathcal{T} \end{aligned} \tag{2.33}$$

then $\hat{\mathbf{Y}} = \mathbf{Y}^\star$ is the unique optimizer to Eq. (2.27) [24].

Yang *et al.* [24] show that, under the conditions of Theorem 2.2.2, one is able to construct such a dual polynomial, thereby proving that $\hat{\mathbf{Y}} = \mathbf{Y}^\star$ is the unique optimizer of the atomic norm minimization problem. Since $Q(f)$ is a function of the frequency, we can retrieve the frequencies of the signal with infinite precision.

Similar to the SMV case, the frequencies can also be retrieved from the optimal Toeplitz matrix by means of a subspace based method.

2.2.3. Performance of the Atomic Norm Minimization Methods

In this section, we show some simulation results to show the difference in performance between the SMV and MMV case. We are interested if and when the MMV case outperforms the SMV case. We are also interested for what values of α (the parameter that is related to the frequency separation) the atomic norm is still able to reconstruct the frequencies perfectly.

First we rewrite the model in Eq. (2.25) as

$$\begin{aligned}\mathbf{Y} &= \sum_{n=1}^{N} c_n \mathbf{a}(f_n, \boldsymbol{\phi}_n), \quad c_n > 0, \mathbf{a}(f_n, \boldsymbol{\phi}_n) \in \mathcal{A} \\ &= \sum_{n=1}^{N} c_n \mathbf{a}(f_n) \boldsymbol{\phi}_n \\ &= \sum_{n=1}^{N} \mathbf{a}(f_n) \mathbf{s}_n, \quad \mathbf{s}_n = [s_{n,1}, \dots, s_{n,L}] = c_n \boldsymbol{\phi}_n \\ &= \mathbf{AS}\end{aligned} \tag{2.34}$$

where $\mathbf{A} = [\mathbf{a}(f_1), \dots, \mathbf{a}(f_N)] \in \mathbb{C}^{|\mathcal{J}| \times N}$, the vector $\mathbf{a}(f_n)$ has elements $a_i(f_n) = e^{j2\pi i f_n}$ and where $\mathbf{S} \in \mathbb{C}^{N \times L}$.

We simulate the model in Eq. (2.34). We solve Eq. (2.14) for the SMV case and Eq. (2.28) for the MMV case. For the SMV case measurement vector $\mathbf{y}$ is the first column of $\mathbf{Y}$, i.e. $\mathbf{y} = \mathbf{Y}_{:,1}$. We take the full data case, $\mathcal{T} = \mathcal{J} = \{0, 1, \dots, M-1\}$ with $M = 20$. For the MMV case $L = 5$. Each iteration we change the frequency separation $\Delta_f = \frac{\alpha}{M-1}$, where we change $\alpha \in \{0.5, 0.55, 0.60, \dots, 2\}$. The frequencies are generated to be equispaced on the interval $[-0.5, 0.5)$, with frequency separation (wrap around distance) Δ_f. We say the signal is recovered with success if the amount of retrieved frequencies $\hat{N}$ is equal to the actual amount of frequencies in the signal N, $\hat{N} = N$, and if additionally the root mean squared error (RMSE) is smaller than $\epsilon = 10^{-5}$, where ϵ is chosen empirically,

$$\text{RMSE} = \sqrt{\frac{1}{N} \sum_{n=1}^{N} (\hat{k}_n - k_n)^2} < \epsilon. \tag{2.35}$$

We will simulate the signal model in Eq. (2.34) for two different source matrices $\mathbf{S}$,

$$\mathbf{S}_1 = \begin{bmatrix} s_1 \\ s_2 \\ \vdots \\ s_N \end{bmatrix} \begin{bmatrix} s_{N+1} & s_{N+2} & \cdots & s_{N+L} \end{bmatrix}, \quad s_i \sim \mathcal{CN}(0,1), \forall i \in \{1, 2, \dots, N+L\} \tag{2.36}$$

and

$$\mathbf{S}_2 \in \mathbb{C}^{N \times L}, \quad s_{n,l} \sim \mathcal{CN}(0,1), \forall n \in \{1, 2, \dots, N\}, \forall l \in \{1, 2, \dots, L\}. \tag{2.37}$$

The columns of $\mathbf{S}_1$ are dependent and as a result also the columns of $\mathbf{Y}_1 = \mathbf{AS}_1$ will be dependent, while the columns of $\mathbf{S}_2$ are independent and as a result also the columns of $\mathbf{Y}_2 = \mathbf{AS}_2$ will be independent. The probability of successful recovery, averaged over 50 Monte Carlo runs, for both cases is shown in Fig. 2.2.

From the figure it is clear that the MMV outperforms the SMV only if the columns are independent. This makes sense as adding an extra column to $\mathbf{y}$ which is a scaled version of $\mathbf{y}$ does not add information. If, however, the columns of $\mathbf{Y}$ are independent, we do add information and therefore the MMV case outperforms the SMV case in practice.

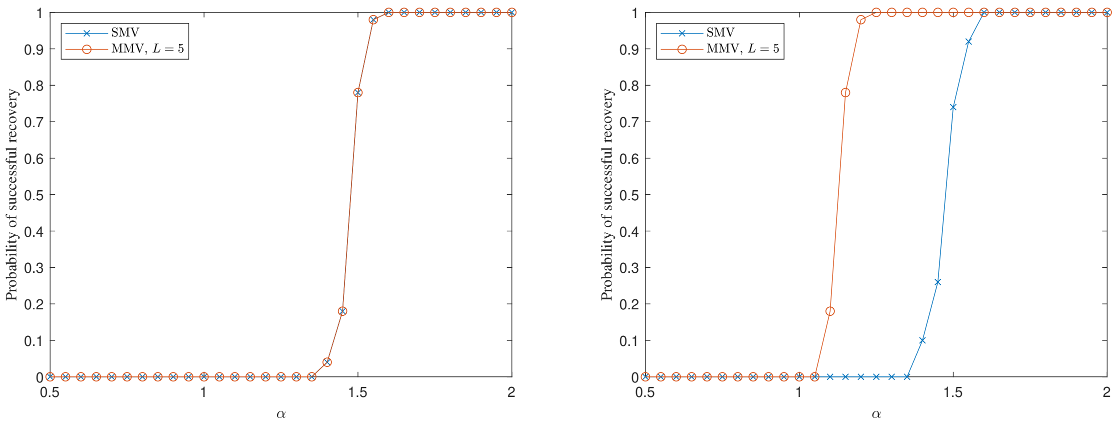

(a) $\mathbf{S}_1$, dependent columns.

(b) $\mathbf{S}_2$, independent columns.

Figure 2.2: The SMV case and the MMV case, simulated for $M = 20$ samples with equispaced frequencies. The probability of successful recovery is averaged over 50 Monte Carlo runs.

2.3. Summary

In this chapter we have covered the theoretical background on two topics. First we discussed the fundamentals of sound field reconstruction. We show that a sound field in an enclosed space can be expanded into room modes and derive an expression for the sound field. Secondly we introduced the atomic norm for the SMV and the MMV case. The MMV case allows for an extra dimension, which can be used to include more measurements. The MMV case outperforms the SMV case in terms of achievable frequency separation only when the extra measurement vectors are independent.

3

Gridless framework for room mode estimation

In this chapter we start the analysis of a gridless framework as replacement for on-the-grid methods for the sound field reconstruction. In Section 3.1 we first define a signal model, then in Section 3.2 we show an on-the-grid method, finally in Section 3.3 we investigate the use of a gridless framework.

3.1. Signal Model for a Sound Field in a 1D Room

In this section, we will define a noiseless signal model for the sound field in the artificial situation of a one-dimensional room with rigid walls.

We will define a signal model for a room that is excited by a source. The main principle is that the source excites the room modes (eigenfunctions) which each have their own spatial frequency (eigenfrequency). In a simple room, i.e. boxed-shaped and with perfectly reflecting rigid walls, the shape of the room modes is a standing wave, thus consisting of a integer number of half-wavelengths. In general, the more complex the shape of the room and the structure of the walls, the more complex the shape of the room modes will be.

In order to reduce the complexity of the problem, we will look at a one-dimensional room with rigid walls. This is a simplified and rather artificial setting. However, its analysis gives insights into the challenges ahead such as the scenarios in higher dimensions and/or with non-rigid walls.

We assume that the room has length L_x and is excited by a point source located at $x = x_0$. The Green's function in this setting is defined as

$$G(x, x_0, \omega) = -\frac{1}{L_x} \sum_{n=0}^{\infty} \frac{\psi_n(x_0)}{(\frac{\omega}{c})^2 - k_n^2} \psi_n(x) \tag{3.1}$$

where c is the speed of sound and $\psi_n(x)$ is the n'th room mode with corresponding n'th modal frequency k_n. Let us assume the source emits L temporal frequencies indicated by ω_l. The sound field is then defined as

$$p(x, \omega) = -\frac{1}{L_x} \sum_{l=1}^{L} C_l \delta(\omega - \omega_l) \sum_{n=0}^{\infty} \frac{\psi_n(x_0)}{(\frac{\omega}{c})^2 - k_n^2} \psi_n(x) \tag{3.2}$$

where $C_l \in \mathbb{R}$ is a constant, which allows for excitation frequencies with varying amplitudes. For a room with rigid walls, $\psi_n(x) = \sqrt{2}\cos(k_n x)$ and $k_n = n\frac{\pi}{L_x}$ [13]. For more details and the derivation of this signal model, the reader is referred to Section 2.1.

In total, we define M_t potential microphone positions inside the room on a uniform grid, i.e., $x_m = \frac{m}{F}$, where $m \in \mathcal{J}_t$ for $\mathcal{J}_t = \{1, 2, \ldots, M_t\}$ and $\frac{1}{F}$ is the distance between successive positions. Note that $x_m \in (0, L_x)$. Similarly, we denote by $\mathcal{J}_o$ the subset of indices corresponding to the observed measurements, i.e., $\mathcal{J}_o \subseteq \mathcal{J}_t$. We place $M_o \leq M_t$ microphones at positions chosen uniformly at random from the index set $\mathcal{J}_t$, to form the 'observed' set. The situation is illustrated in Fig. 3.1. Note that this notation allows for nonuniform microphone allocation.

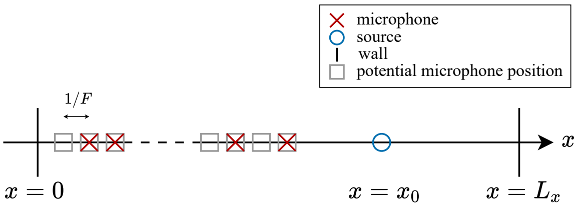

Figure 3.1: Measurement setup in a 1D room.

If we assume we can represent the sound field with a finite number of room modes, the sum in Eq. (3.2) becomes finite. This allows us to write the measurements as a system of equations. Using the complex exponential expansion for the cosine function, we can define a system over the set $\mathcal{J}_t$ as

$$\mathbf{P} = \mathbf{A}\mathbf{S} \tag{3.3}$$

where the potential measurements are stacked in the matrix $\mathbf{P} \in \mathbb{R}^{M_t \times L}$, with columns $\mathbf{p}_l = [p(x_1, \omega_l), \dots, p(x_{M_t}, \omega_l)]^T$. Thus each column represents the measured sound field at a certain excitation frequency. The steering matrix $\mathbf{A}$ adheres to a Vandermonde structure and is defined as $\mathbf{A} = [\mathbf{a}(k_1), \dots, \mathbf{a}(k_N)] \in \mathbb{C}^{M_t \times N}$. Its columns contain the set of modal frequencies, $\mathbf{a}(k_n) = [e^{jk_n x_1}, e^{jk_n x_2}, \dots]^T$, with $n \in \{-\frac{N-1}{2}, \dots, +\frac{N-1}{2}\}$. The matrix $\mathbf{S} \in \mathbb{C}^{N \times L}$ is the source matrix containing the weights of each modal frequency, with elements $s_{n,l} = -\frac{C_l}{L_x} \frac{\cos(k_n x_0)}{(\frac{\omega_l}{c})^2 - k_n^2}$. Note that the source matrix has the structure of the Green's function in Eq. (3.1).

From the measurements, $\mathbf{P}$, we want to retrieve the modal frequencies and their corresponding amplitudes. Note that if the modal frequencies are known and furthermore the source is completely known (its location, its amplitude, etc.), then, with the expression in Eq. (3.2) we can calculate the sound pressure at any point in space for any excitation frequency.

In general this system in Eq. (3.3) is underdetermined, $N > M_t$. However, the columns of the source matrix are approximately sparse, as only the room modes with modal frequencies close to $\frac{\omega_l}{c}$ get excited significantly. This allows for compressive sensing techniques to solve the system of equations.

In the following sections we describe how an existing on-the-grid method and the proposed gridless method are applied to this signal model.

3.2. Existing On-the-grid Method

Prior art (e.g. [4, 5]) uses an on-the-grid method in order to determine the modal frequencies and corresponding amplitudes. Typically they define a discrete dictionary of R spatial frequencies $v_r \in [-\pi F, \pi F]$ on a uniform grid. Using this dictionary, the assumed basis $\mathbf{D}$ is constructed,

$$\mathbf{D} = \begin{bmatrix} e^{jv_1 x_1} & e^{jv_2 x_1} & \dots & e^{jv_R x_1} \\ e^{jv_1 x_2} & \ddots & & \\ \vdots & & & \vdots \\ e^{jv_1 x_{M_t}} & & \dots & e^{jv_R x_{M_t}} \end{bmatrix}. \tag{3.4}$$

Then [4, 5] minimize an ℓ_1-norm of a weighted vector $\mathbf{b}$ and solve the system (excitation) frequency by (excitation) frequency,

$$\begin{aligned} \min_{\mathbf{b}_l \in \mathbb{C}^R} \quad & ||\mathbf{L}_l \mathbf{b}_l||_1 \\ \text{s.t.} \quad & \mathbf{p}_{l,i} - \mathbf{D}_i \mathbf{b}_l = 0, \forall i \in \mathcal{J}_o. \end{aligned} \tag{3.5}$$

Here $\mathbf{p}_{l,i}$ denotes the l'th column and corresponding i'th row element of the matrix $\mathbf{P}$, the weighting matrix is defined as $\mathbf{L}_l = \operatorname{diag}\left(\left(\frac{\omega_l}{c}\right)^2 - \mathbf{v}^2\right)$, with $\mathbf{v} = [v_1, \ldots, v_R]^T$. We change this method slightly such that it is able to solve for multiple excitation frequencies at once, that is,

$$\begin{array}{cl} \underset{[\mathbf{b}_1, \mathbf{b}_2, \ldots, \mathbf{b}_L] \in \mathbb{C}^{R \times L}}{\min} & \sum_l^L ||\mathbf{L}_l \mathbf{b}_l||_1 \\ \text{s.t.} & \mathbf{P}_i - \mathbf{D}_i[\mathbf{b}_1, \mathbf{b}_2, \ldots, \mathbf{b}_L] = 0, \forall i \in \mathcal{J}_o. \end{array} \tag{3.6}$$

The basis mismatch problem results from the discrete dictionary $\mathbf{D}$. As was described in Section 1.4, one assumes that the modal frequencies are inside this dictionary, but in practice this is never exactly the case resulting in a mismatch between the actual basis $\mathbf{A}$ and the assumed basis $\mathbf{D}$. If the size of the dictionary is increased, the mismatch decreases, however this comes with increased computational costs and higher coherence between the columns of $\mathbf{D}$ [20]. If the dictionary is too small, the modal frequencies might not be in the dictionary, decreasing the accuracy of the reconstruction. If an on-the-grid method is used, one thus has to tackle this trade-off but will inherently make an error due to the fact that a grid is used.

In the next section we will therefore look at the atomic norm, a gridless method, that does not suffer from this basis mismatch.

3.3. Proposed Framework using the Atomic Norm

In this section, we investigate the use of a gridless framework, using the atomic norm [7, 24], to circumvent the basis mismatch problem. We directly jump to the multi measurement vector (MMV) case, which allows to solve for multiple excitation frequencies at once. From the MMV case the behaviour of the Single Measurement Vector (SMV) case can be easily obtained by setting $L = 1$. In Section 2.2 a detailed explanation and analysis of the atomic norm is given, including both the SMV and the MMV case.

The atomic norm makes use of a set of atoms as dictionary,

$$\mathcal{A} = \{\mathbf{a}(f, \boldsymbol{\phi}) = \mathbf{a}(f)\boldsymbol{\phi} \ : f \in [0, F), \boldsymbol{\phi} \in \mathbb{C}^{1 \times L}, ||\boldsymbol{\phi}||_2 = 1\} \tag{3.7}$$

where $\mathbf{a}(f) = [e^{j2\pi f x_1}, \ldots, e^{j2\pi f x_{M_t}}]^T \in \mathbb{C}^{M_t}$. Note that the frequency f is defined over a continuous interval, therefore the set defines a continuous dictionary. The atomic (ℓ_1) norm is defined as

$$||\mathbf{P}||_{\mathcal{A}} = \inf\Big\{ \sum_{k \in \mathcal{K}} c_k : \mathbf{P} = \sum_{k \in \mathcal{K}} c_k \mathbf{a}(f_k, \boldsymbol{\phi}_k), \ \mathbf{a}(f_k, \boldsymbol{\phi}_k) \in \mathcal{A} \Big\} \tag{3.8}$$

where $c_k > 0$ and $\mathcal{K}$ is the set containing the indices of the atoms. As an alternative to the on-the-grid method in (3.6), we use the atomic norm to promote a sparse set of modal frequencies:

$$\min_{\tilde{\mathbf{P}} \in \mathbb{C}^{M_t \times L}} ||\tilde{\mathbf{P}}||_{\mathcal{A}}, \text{ s.t. } \tilde{\mathbf{P}}_i = \mathbf{P}_i, \quad \forall i \in \mathcal{J}_o. \tag{3.9}$$

The atomic norm can be cast into an SDP [7]. Therefore the optimization problem is reformulated as

$$\begin{array}{cl} \underset{\mathbf{W} \in \mathbb{C}^{L \times L}, \mathbf{u} \in \mathbb{C}^{M_t}, \tilde{\mathbf{P}} \in \mathbb{R}^{M_t \times L}}{\min} & \operatorname{Tr}(\operatorname{Toep}(\mathbf{u})) + \operatorname{Tr}(\mathbf{W}) \\ \text{s.t.} & \begin{bmatrix} \operatorname{Toep}(\mathbf{u}) & \tilde{\mathbf{P}} \\ \tilde{\mathbf{P}}^H & \mathbf{W} \end{bmatrix} \succcurlyeq 0 \\ & \tilde{\mathbf{P}}_i = \mathbf{P}_i, \quad \forall i \in \mathcal{J}_o. \end{array} \tag{3.10}$$

Using the matrix $\operatorname{Toep}(\mathbf{u})$, the atomic norm tries to find a matrix related to the covariance matrix of $\mathbf{P}$. From the optimal solution $\operatorname{Toep}(\hat{\mathbf{u}})$, we can therefore retrieve the estimated frequencies using any subspace method. Assume that the $\boldsymbol{\phi}_k$'s are independent random variables with $\mathbb{E}[\boldsymbol{\phi}_k] = \mathbf{0}$. Then, if the modal frequencies k_n adhere to a certain frequency separation,

$$\Delta_k \geq 2\pi F \frac{\alpha}{M_t - 1} \tag{3.11}$$

there exists a numerical constant C, such that

$$M_o \geq C \max \left\{ \log^2 \frac{M_t\sqrt{L}}{\delta}, N \log \frac{N}{\delta} \log \frac{M_t\sqrt{L}}{\delta} \right\} \tag{3.12}$$

is sufficient to guarantee that, with probability at least $1-\delta$, the atomic norm will exactly recover the original signal [7]. Tang *et al.* [7] proved that successful recovery of the (modal) frequencies is guaranteed if $\alpha = 4$ in (3.11). However in practice its value can be lower [24], and depends on the parameters of the model. Note that our model in Eq. (3.3) only approximately meets all the assumptions on $\boldsymbol{\phi}_k$, as the rows of $\mathbf{S}$ are not completely independent. It is therefore of great interest to look at the performance of the atomic norm for our signal model, and to derive corresponding bounds on the value of α.

3.3.1. Bound from Modal Frequencies Separation

The modal frequencies in a one-dimensional room with rigid walls are given by $k_n = n\frac{\pi}{L_x}$ (see section 2.1 and [13]). The frequency separation is thus $\Delta_k = \frac{\pi}{L_x}$. Using this, we can rewrite (3.11) and derive that we need at least

$$\begin{aligned} M_t &\geq 2\pi F \frac{\alpha}{\Delta_k} + 1 \\ &= 2 \cdot F \cdot \alpha \cdot L_x + 1. \end{aligned} \tag{3.13}$$

However, due to the fact that we have spatial measurements, there is a limitation to the number of measurements. The size of the room puts a limit to the number of possible measurement locations M_t; the measurements must be inside the room, thus $0 < x_m < L_x, \forall m \in \mathcal{J}_t$. Therefore we must have that $\min_m(x_m) = \frac{1}{F} > 0$, which is satisfied, and that

$$\max_m(x_m) = \frac{M_t}{F} < L_x \tag{3.14}$$

and thus

$$M_t < F \cdot L_x. \tag{3.15}$$

Now we combine (3.13) and (3.15), to write

$$F \cdot \alpha \cdot 2L_x + 1 < F \cdot L_x. \tag{3.16}$$

The inequality in (3.16) will be satisfied for practical situations ($L_x > 0, F > 0$) if and only if $\alpha < \frac{1}{2}$. Although, in practice, the value of α is determined by the performance of the atomic norm, as we will see in Chapter 5, we can discuss which value of α is desired. The situation is illustrated in Fig. 3.2. It shows a plot of the left hand side (orange $\alpha = 2$, yellow $\alpha = 0.4$) and the right hand side (blue) of Eq. (3.16) as a function of the room length L_x. The figure can be interpreted as follows. The blue line is the amount of samples that one can fit inside the room, where F determines the Nyquist sampling rate. The orange and the yellow lines indicate the amount of samples that one needs in order to reach the frequency separation, determined by α. Therefore we require $\alpha < \frac{1}{2}$. Note that the gap between the lines increases with the length of the room. This is expected as both the frequency separation of the modal frequencies and the number of possible measurements depend on the length of the room.

In conclusion, the frequency separation required by the atomic norm, shown in (3.11), has to reach at least $\alpha < \frac{1}{2}$, in order to be able to solve the modal frequency estimation problem exactly. Now, before we look at the performance of the atomic norm in practice in Chapter 5, we first derive a lower bound for α that is inherent to the problem itself.

3.3.2. Bound from Known vs. Unknown Variables

Due to the fact that only a finite number of measurements is available in practice, the estimated modal frequencies cannot be arbitrarily close. We are interested in a lower bound on the frequency separation, regardless of the method one is using to solve the problem. We can then relate this bound to the frequency separation required by the atomic norm, to get an idea of the performance of the atomic norm.

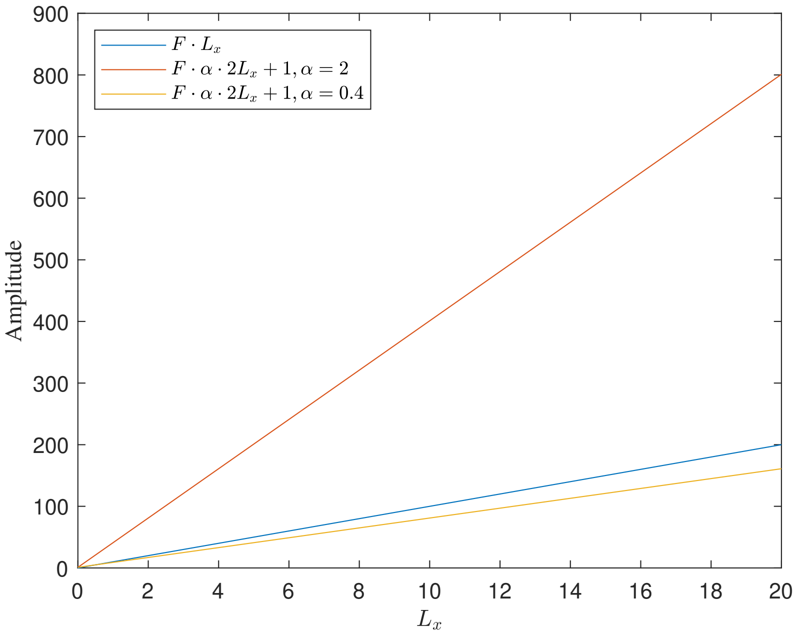

Figure 3.2: Amplitude of left and right hand side of Eq. (3.16) as a function of the room length L_x for $F = 10$, where $\frac{1}{F}$ is the distance between two consecutive microphone positions.

From Eq. (3.3) we know that we have M_tL known variables, the number of (real) elements in the measurement matrix $\mathbf{P}$. On the contrary, the steering matrix $\mathbf{A}$ and the source matrix $\mathbf{S}$ are unknown, resulting in $N(1+L)$ unknown variables in total; N unknown frequencies in $\mathbf{A}$ (not M_tN because the structure of $\mathbf{A}$ is assumed to be known), and NL unknown variables in $\mathbf{S}$ (of which the structure is not known). If no other prior knowledge is available, we require more known variables than unknown variables, that is,

$$M_tL \geq N(1+L) \tag{3.17}$$

and thus,

$$\frac{1}{N} \geq \frac{(1+L)}{M_tL}. \tag{3.18}$$

Note that if N (spatial) frequencies are to be fit uniformly on a interval of length $2\pi F$, then the maximum frequency separation that can be reached is $\frac{2\pi F}{N}$, thus $\frac{2\pi F}{N} = 2\pi F \frac{\alpha}{M_t - 1}$. As a result, and using (3.18),

$$\begin{aligned} \alpha &= (M_t - 1)\frac{1}{N} \geq (M_t - 1)\frac{(1+L)}{M_tL} \\ &= (1 + \frac{1}{L})(1 - \frac{1}{M_t}). \end{aligned} \tag{3.19}$$

From (3.19) it is clear that α will always be greater than the desired maximum value $\frac{1}{2}$, provide that $L > 0$ and $M_t > 1$. Thus, we can conclude that the frequency separation required by the atomic norm cannot be reached, by construction of the problem.

This means that more prior knowledge about the problem has to be included. This can be done by either increasing the number of known variables or decreasing the number of unknown variables, such that the bound derived in (3.19) can be lowered.

3.4. Summary

In this chapter we have investigated whether we can use a gridless framework for estimating the room modes of a sound field in a one-dimensional room with rigid walls. The main contributions in this chapter are summarized as follows:

- A signal model of the sound field in a one-dimensional room with rigid walls is defined.
- The optimization problem that is used by prior art as an on-the-grid method is stated and its basis mismatch problem is briefly discussed.
- The gridless method using the atomic norm is proposed as an alternative. We derived two bounds for the frequency separation in the signal. One upper bound that is required by the separation of the modal frequencies or room modes, and one lower bound following from the number of known variables and unknown variables. If no additional prior knowledge is added to the problem, the lower bound is larger than the upper bound, resulting in a feasibility problem.

Although we have gained insight into how a gridless framework would behave, can conclude that the current framework is not yet suited for estimating room modes. As a provisional and partial answer to the research question RQ.1, we can thus state that, without prior knowledge we cannot formulate a gridless framework that can successfully recovery the modal frequencies. More prior knowledge, e.g. knowledge on the shape of the room modes, has to be included in the problem.

In the next chapter we will continue to look for an answer to the research question RQ.1. We will investigate how to exploit prior knowledge about the sound field, which may result in a better performance of the proposed framework.

4

Exploiting Prior Knowledge

In the previous chapter we showed that more prior knowledge is required for perfect reconstruction by the atomic norm. In this chapter we discuss multiple ways to exploit prior knowledge, and analyze its effect on the bounds derived in the previous chapter. In each section we add or change something to the framework of the optimization problem in Eq. (3.10)*, such that all the ways to exploit the prior knowledge are combined in the final section of this chapter.*

4.1. Shape of the Steering Matrix

For a 1D room with rigid walls the room modes are known to be of the form

$$\psi_n(x) = \sqrt{2}\cos(k_n x), \quad k_n = n\frac{\pi}{L_x}. \tag{4.1}$$

Since the cosine function consists of a negative and a positive frequency, the (spatial) frequencies in the steering matrix $\mathbf{A}$ are symmetric around zero. We would like to incorporate this knowledge into the problem.

Note that the columns of $\mathbf{A}$ can be shifted around, without changing the signal $\mathbf{P}$, if the rows of $\mathbf{S}$ are shifted accordingly. Without loss of generality, we can thus sort the frequencies in $\mathbf{A}$ such that the columns are symmetric around the zero frequency,

$$A = \begin{bmatrix} \dots & \mathbf{a}(-f_2) & \mathbf{a}(-f_1) & \mathbf{a}(0) & \mathbf{a}(f_1) & \mathbf{a}(f_2) & \dots \end{bmatrix}. \tag{4.2}$$

Additionally, by choosing the potential microphone positions, specified by $\mathcal{J}_t$, the structure of $\mathbf{A}$ can be influenced. Suppose we measure symmetrically around $x = 0$. For example, let $\mathcal{J}_t = \{-1, 0, 1\}$ and we only consider the first three room modes (thus $N = 5, n \in \{-2, -1, 0, 1, 2\}$). The steering matrix can then be written as

$$A = \begin{bmatrix} e^{-jk_2} & e^{-jk_1} & 1 & e^{jk_1} & e^{jk_2} \\ 1 & 1 & 1 & 1 & 1 \\ e^{jk_2} & e^{jk_1} & 1 & e^{-jk_1} & e^{-jk_2} \end{bmatrix}. \tag{4.3}$$

Note that $\mathbf{A}$ is now a so called centro-symmetric matrix; its elements are symmetric around the centre element of the matrix. A formal definition of a centro-symmetric matrix is given in Definition 4.1.1.

Definition 4.1.1. *A matrix* $\boldsymbol{A} \in \mathbb{C}^{M\times N}$ *is centro-symmetric if and only if* $\boldsymbol{\Pi}_M \boldsymbol{A} \boldsymbol{\Pi}_N = \boldsymbol{A}$*, where* $\boldsymbol{\Pi} \in \{0,1\}^{M\times M}$ *and* $\boldsymbol{\Pi} \in \{0,1\}^{N\times N}$ *are permutation matrices with ones on the anti-diagonals.*

Moreover, note that the following equations are equivalent

- $\mathbf{\Pi}_M \mathbf{A} \mathbf{\Pi}_N = \mathbf{A}$,
- $\mathbf{\Pi}_M \mathbf{A} = \mathbf{A} \mathbf{\Pi}_N$,
- $\mathbf{A}^H \mathbf{\Pi}_M = \mathbf{\Pi}_N \mathbf{A}^H$,
- $\mathbf{\Pi}_M \mathbf{A} \mathbf{A}^H \mathbf{\Pi}_M = \mathbf{A} \mathbf{A}^H$.

For the rigid walls case we know beforehand that the frequencies are symmetric around zero and we would thus like to constrain the minimization problem (Eq. (3.10)), such that the solution space is limited by the sets of symmetric frequencies. Ideally we would add the equality constraint

$$\mathbf{\Pi}_M \mathbf{A} \mathbf{\Pi}_N = \mathbf{A}. \tag{4.4}$$

However, the steering matrix $\mathbf{A}$ is unknown, as it contains the frequencies which we are trying to find. For this reason we propose to constrain the Toeplitz matrix as follows.

We know that the optimal value is $\mathrm{Toep}(\hat{\mathbf{u}}) = \hat{\mathbf{T}} = \mathbf{A}\mathbf{Z}\mathbf{A}^H$, where the matrix $\mathbf{Z} \in \mathbb{R}^{+N \times N}$ is a diagonal matrix with on its diagonal the magnitudes of rows of the source matrix $\mathbf{S}$,

$$\mathbf{Z} = \begin{bmatrix} ||\mathbf{S}_{-\frac{N-1}{2}}||_2 & & \mathbf{0} \\ & \ddots & \\ \mathbf{0} & & ||\mathbf{S}_{+\frac{N-1}{2}}||_2 \end{bmatrix}. \tag{4.5}$$

We thus investigate what happens if we force $\hat{\mathbf{T}}$ to be centro-symmetric. We start by writing,

$$\mathbf{\Pi}_M \hat{\mathbf{T}} \mathbf{\Pi}_M = \mathbf{\Pi}_M \mathbf{A}\mathbf{Z}\mathbf{A}^H \mathbf{\Pi}_M = \mathbf{A} \mathbf{\Pi}_N \mathbf{Z} \mathbf{\Pi}_N \mathbf{A}^H. \tag{4.6}$$

Thus, if $\mathbf{Z}$ is centro-symmetric, then $\hat{\mathbf{T}}$ is centro-symmetric too. For $\mathbf{Z}$ to be centro-symmetric, the rows of $\mathbf{S}$ must satisfy that $||\mathbf{S}_{-n}||_2 = ||\mathbf{S}_n||_2$.

If we look at the elements of the source matrix for the rigid wall case,

$$\mathbf{S}_{n,l} = \frac{\psi_n(x_0)}{(\frac{\omega_l}{c})^2 - k_n^2} \tag{4.7}$$

we see that there is symmetry in the rows of the source matrix, i.e. $\mathbf{S}_{-n} = \mathbf{S}_n$, thus the powers of these rows will also be equal. Therefore, in the rigid walls case, the matrix $\mathbf{Z}$ will be centro-symmetric.

The proposed minimization problem is therefore,

$$\begin{aligned} \min_{\mathbf{W} \in \mathbb{C}^{L \times L}, \mathbf{u} \in \mathbb{C}^{M_t}, \tilde{\mathbf{P}} \in \mathbb{R}^{M_t \times L}} \quad & \mathrm{Tr}(\mathrm{Toep}(\mathbf{u})) + \mathrm{Tr}(\mathbf{W}) \\ \text{s.t.} \quad & \begin{bmatrix} \mathrm{Toep}(\mathbf{u}) & \tilde{\mathbf{P}} \\ \tilde{\mathbf{P}}^H & \mathbf{W} \end{bmatrix} \succcurlyeq 0 \\ & \tilde{\mathbf{P}}_i = \mathbf{P}_i, \quad \forall i \in \mathcal{J}_o \\ & \mathbf{\Pi}_M \mathrm{Toep}(\mathbf{u}) \mathbf{\Pi}_M = \mathrm{Toep}(\mathbf{u}). \end{aligned} \tag{4.8}$$

We note that the centro-symmetric constraint on $\mathrm{Toep}(\mathbf{u})$ is the same forcing $\mathbf{u}$ to be real. However, the centro-symmetric constraint does give some more insight in what is changed in the optimization problem, and therefore gives a solid motivation to change the solution space of $\mathbf{u}$.

Unfortunately, forcing the vector $\mathbf{u}$ to be real means that only the solution space is made smaller. Thus, if the optimal solution is already in the smaller solution space, then forcing the vector $\mathbf{u}$ to be real will not improve performance. It will have no effect on the bounds derived in Section 3.3. At most it can speed up the solving process, but that depends on the initialization point of the algorithm that is solving the minimization problem. This expected behaviour is verified by simulations in Chapter 5.

4.2. Mirror Image Model

As was shown in Section 3.3, using only the measurements inside the room is not enough to achieve the frequency separation required by the atomic norm for successful recovery. In this section, we will increase the number of measurements, and thus the number of known variables, with a factor two, by including the reflections of the wall.

One way of adding measurements is to make use of the geometry of the room; we can make use of the symmetry with respect to the walls. Each wall reflects the sound field, produced by the source, as if there is a virtual source behind the wall. Modeling these virtual sources to compute the reflections is called the mirror image source method [25]. If we consider the rigid walls case, the virtual sources even have the same amplitude and phase as the real source. Reasoning along the same lines, it follows that also the microphones can be copied into the virtual rooms behind the walls. An example of the resulting measurements for a 1D room with a mirror image in the left wall is shown in Fig. 4.1.

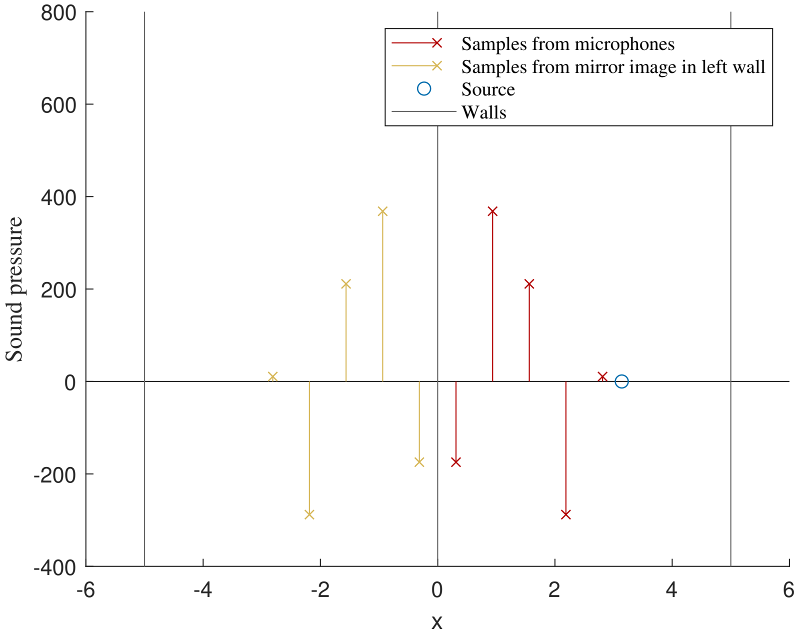

Figure 4.1: Measurements including mirror image in left wall, in the case of rigid walls, $L_x = 5$.

In theory, we could add as many virtual rooms to the left and right of our real room, to get an arbitrarily high amount of samples. However, there are two things we want to point out here.

First of all, only the first room on the left and the first room on the right actually add information, as these reflections tell that the sound field has symmetry with respect to the left and right wall. By adding more rooms, no additional information is given, as the same symmetry with respect to the same walls is used to construct the samples in these rooms. Thus by adding the second (or third, fourth, etc.) reflections, we only add extra samples, we do not add extra information.

Secondly, for the 'mirror' operation, the location of the corresponding wall must be known. We could create images in both walls, however, this would mean we know the length of the room. Since we look at the rigid wall case, the length of the room solely determines the modal frequencies ($k_n = n\frac{\pi}{L_x}$). Mirroring in both walls would mean we are looking for something we assume we already know. In order to avoid such a trivial case, we assume the length of the room is not fully known, i.e., we only take as reference one of the walls and use it to duplicate the measurements by mirroring them.

Note that the real and the virtual measurements together will generally not be on a uniform grid anymore. However, the structure of the atomic norm allows us to fill up the grid with unknown samples to form a uniform grid again, indicated by dashed squares in Fig. 4.2. We could also place the measurements in such a way that, together with the virtual samples, they directly form a uniform grid. In that case the distance between the wall and the closest microphone must be exactly $\frac{1}{2F}$.

The mirrored measurements are constructed as follows,

$$\mathbf{P}_{\text{mirror image}} = \mathbf{\Pi}_{M_t}\mathbf{P}^*. \tag{4.9}$$

Here the permutation matrix is used to 'flip' the location of the measurements, and the complex conjugate operator is used to flip the frequencies. The minimization problem in Eq. (3.10) can be altered such that it inherits also the mirror image.

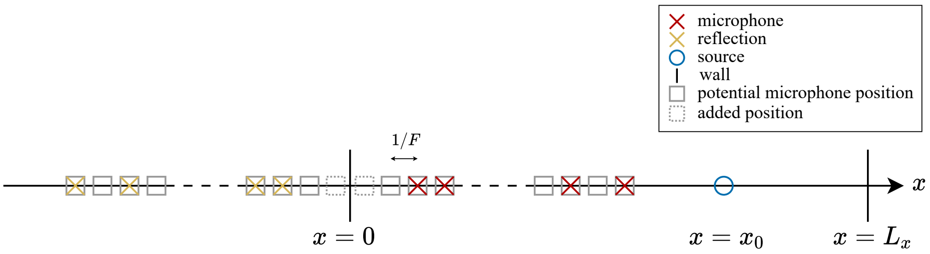

Figure 4.2: Measurement setup in a 1D room, including the virtual measurements (in yellow) obtained from the mirror image and the added positions (dotted in gray) to form a uniform sampling grid.

$$
\begin{aligned}
\min_{\mathbf{W}\in\mathbb{C}^{L\times L},\mathbf{u}\in\mathbb{R}^{2M_t},\tilde{\mathbf{P}}\in\mathbb{R}^{2M_t\times L}} \quad & \mathrm{Tr}(\mathrm{Toep}(\mathbf{u}))+\mathrm{Tr}(\mathbf{W}) \\
\text{s.t.} \quad & \begin{bmatrix}\mathrm{Toep}(\mathbf{u}) & \tilde{\mathbf{P}} \\ \tilde{\mathbf{P}}^H & \mathbf{W}\end{bmatrix} \succcurlyeq 0 \\
& \tilde{\mathbf{P}}_i = \begin{bmatrix}\mathbf{\Pi}_{M_t}\mathbf{P}^* \\ \mathbf{P}\end{bmatrix}_i, \forall i \in \mathcal{J}_o.
\end{aligned} \tag{4.10}
$$

Note the slight abuse of notation in (4.10), as the index i now indicates two rows, due to the construction of the mirrored measurements.

By including one reflection, the number of knowns is increased by a factor two, therefore the lower bound on α becomes

$$\alpha \geq \frac{1}{2}(1+\frac{1}{L})(1-\frac{1}{M}). \tag{4.11}$$

By adding these new measurements, we have managed to reduce the constraint on the number of measurements. However, we still need to further exploit the structure of the problem in addition to the mirror image to meet the inequality in (3.16).

4.3. Spectral Symmetry

In Section 4.1 we showed how to shrink the solution space of the optimization problem such that the optimal solution can only consist of cosines. In this section, we will make use of the Hilbert transform to remove the negative part of the frequency spectrum, such that the number of unknown frequencies decreases by a factor two.

Due to the room modes being cosines, all positive modal frequencies will also occur on the negative side of the spatial frequency spectrum. In theory we only need to estimate half of the frequencies, either the positive or the negative part, as the other half follows directly.

To reduce the number of unknowns, we would thus like to remove the negative (or positive) side of the spectrum in our signal. This can be done by using the discrete or continuous Hilbert transform. However, the discrete Hilbert transform will have a very poor resolution due to the low amount of (spatial samples) that is typically available. Since high (or actually infinite) resolution is precisely what we aim to achieve with the atomic norm, the discrete Hilbert transform is not useful.

The continuous Hilbert transform of a function $f(t)$ is given by

$$H(f)(t) = \frac{1}{\pi t} * f(t) \tag{4.12}$$

where '$*$' denotes the convolution sign. The Hilbert transform of the cosine function is $H(\cos)(t) = \sin(t)$ [26]. This can be used to remove the negative frequencies. Suppose $f(t) = \cos(t)$, we can write

$$f_a(t) = f(t) + jH(f)(t) = \cos(t) + j\sin(t) = e^{jt}. \tag{4.13}$$

We have used the subscript 'a' because the function $f_a(t)$ is often called the analytic function. The function $f_a(t)$ now only contains the positive frequency of $f(t)$.

Note that we need a continuous signal in order to be able to apply the continuous Hilbert transform. To create continuous signal, one could use a moving microphone instead of a static grid of microphones. Suppose the microphone is traveling with a constant speed v, the variable x in the signal model in (3.2) is replaced by vt to get a continuous measurement in time [27]. On the downside, as the microphone is moving during acquisition of the measurements, the Doppler effect comes into play. However it was shown that this effect can be removed again [28]. A sampling scheme with a moving microphone has some more advantages over the static sampling scheme, for a detailed discussion the interested reader is referred to [27, 28].

Summarizing, we would have to use a moving microphone to get a continuous signal. First, the Hilbert transform is applied to the continuous signal, then the signal is discretized again, by $t_m = \frac{1}{v}x_m$, such that the notation is consistent. An overview of the acquisition method is shown in Fig. 4.3. The practical implementation of the acquisition method is out of scope of this work. For the remaining part of this work we assume that it is possible to remove the negative (spatial) frequencies from the measured sound field.

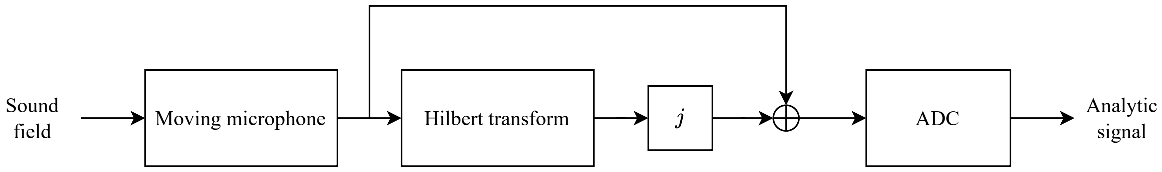

Figure 4.3: Block diagram of the acquisition method using a moving microphone in order to remove the negative frequencies in the measured sound field.

Inspired by [29], we introduce an extra constraint to the minimization problem, to ensure the proposed framework finds a solution consisting of only positive frequencies. Assuming the negative frequencies are removed, the new optimization problem is shown in Eq. (4.14). The frequency interval to which the solution is bounded is given by $k \in [a-b, a+b]$.

$$\begin{aligned} \min_{\mathbf{W}\in\mathbb{C}^{L\times L},\mathbf{u}\in\mathbb{C}^{2M_t},\tilde{\mathbf{P}}\in\mathbb{R}^{2M_t\times L}} \quad & \mathrm{Tr}(\mathrm{Toep}(\mathbf{u})) + \mathrm{Tr}(\mathbf{W}) \\ \text{s.t.} \quad & \begin{bmatrix} \mathrm{Toep}(\mathbf{u}) & \tilde{\mathbf{P}} \\ \tilde{\mathbf{P}}^H & \mathbf{W} \end{bmatrix} \succcurlyeq 0 \\ & \tilde{\mathbf{P}}_i = \begin{bmatrix} \mathbf{\Pi}_{M_t}\mathbf{P}^* \\ \mathbf{P} \end{bmatrix}_i, \forall i \in \mathcal{J}_o \\ e^{-ja}\mathbf{F}\mathrm{Toep}(\mathbf{u})\mathbf{G}^H + & e^{ja}\mathbf{G}\mathrm{Toep}(\mathbf{u})\mathbf{F}^H \\ & -2\cos(b)\mathbf{G}\mathrm{Toep}(\mathbf{u})\mathbf{G}^H \succcurlyeq 0. \end{aligned} \tag{4.14}$$

Here $\mathbf{\Pi}_{M_t}$ is a permutation matrix with ones on its anti-diagonal, and zeros elsewhere, $a = b = \frac{\pi}{2}$ and

$$\mathbf{F} = \begin{bmatrix} \mathbf{0}_{(M_t-1),1} & \mathbf{I}_{M_t-1} \end{bmatrix}, \tag{4.15}$$

$$\mathbf{G} = \begin{bmatrix} \mathbf{I}_{M_t-1} & \mathbf{0}_{(M_t-1),1} \end{bmatrix}. \tag{4.16}$$

Note again the slight abuse of notation in (4.14), as the index i indicates two rows, due to the construction of the mirrored measurements. More over, the solution space for the parameter $\mathbf{u}$ is changed back to the complex numbers, because by removing the negative frequencies, we obviously lose the spectral symmetry in the signal.

By performing the Hilbert transform, the number of unknowns is decreased by a factor two, therefore the lower bound on α becomes

$$\alpha \geq \frac{1}{4}(1+\frac{1}{L})(1-\frac{1}{M}). \tag{4.17}$$

Now the lower bound is smaller than $\frac{1}{2}$. Hence, the remaining question is whether the atomic norm attains a value lower than $\frac{1}{2}$ in practice.

4.4. Summary

In this chapter we have investigated multiple methods to incorporate prior knowledge into the minimization problem. We list the methods that have been covered:

- The fact that the sound field is symmetrical in its spatial frequency domain was used to shrink the solution space of the optimization problem. Unfortunately, this cannot be used to decrease the lower bound on α.
- The reflection in the walls was used to create extra virtual measurements. The lower bound on α can therefore be decreased by a factor two.
- Finally the continuous Hilbert transform was used to remove the negative modal frequencies in the signal. Using this, the lower bound on α can then again be decreased by a factor two.

We have now created a framework, exploiting prior knowledge of the sound field, such that the discrepancy between the two bounds derived in the Chapter 3 is removed. This means that the atomic norm could in theory solve the problem exactly, and thus we have a good prospect to answer the research question Eq. (RQ.1) positively. However, the remaining question is whether the atomic norm attains the lower bound in practice. Its success is thus not yet guaranteed, as the atomic norm does not have to attain the lower bound per se.

In the next chapter we will investigate the performance of the gridless framework.

5

Simulation Results

In this chapter we verify the bounds derived in Chapter 3 and investigate the effect of including prior knowledge as described in Chapter 4 with numerical simulations. We first introduce two simulation methods that are used for the analysis in Section 5.1. Then, we simulate the framework with and without exploiting prior knowledge in Section 5.2 and Section 5.3 respectively.

5.1. Simulation Methods

In this section, we discuss the simulation methods that are used to analyze and compare the performance of the different version of the proposed framework, as describe in the previous chapters (Chapters 3 and 4).

5.1.1. Dual Polynomial

First of all we use the dual polynomial to analyze the performance of the frequency retrieval. The dual polynomial can be computed from the dual problem of the optimization problem and can easily be obtained using any off-the-shelf solver in Matlab. As discussed in Chapter 2, the dual polynomial is a function $Q(k) : [-\pi F, \pi F) \to \mathbb{C}$. Its magnitude will attain the value one exactly at the retrieved frequencies. The magnitude of a dual polynomial as a function of frequency is shown in Fig. 5.1 for illustration. In Fig. 5.1a the function attains the value one exactly at the indicated frequencies, thus the atomic norm successfully recovers the frequencies, where in Fig. 5.1b it does not have success.

The dual polynomial gives some useful insights. To some extent, one can see how close the atomic norm is to perfect reconstruction, due to the location of the peaks. Secondly, the height of the "side lobes" indicate how robust the framework is against interference; the lower the side lobes, the higher the robustness. The dual polynomial can thus be used to get inside in the quality of the reconstruction.

5.1.2. Frequency Separation

We want to be able to verify the derived bounds and to be able to compare different methods quantitatively. Therefore we look at the probability of successful recovery with respect to the frequency separation as a function of α. We thus simulate the model as described by Eq. (3.3). However, we change the set of modal frequencies to $k_n = n \cdot 2\pi F \frac{\alpha}{M_t - 1}$. Therefore the results from this method will not represent physical rooms anymore, but are purely used to evaluate the derived bounds. The frequency separation in the signal is changed each step by changing α. For each α we solve the optimization problem and look if it has a successful recovery of the frequencies. We assume the source emits L frequencies, which are i.i.d. from $\mathcal{U}[0, c\pi F)$. This range corresponds to the Nyquist range for the modal frequencies. The idea is that on average all the modal frequencies have an equal chance to be excited.

We say the signal is recovered with success if two conditions are satisfied. First of all, the number of retrieved modal frequencies $\hat{N}$ must be equal to the actual number of modal frequencies in the signal

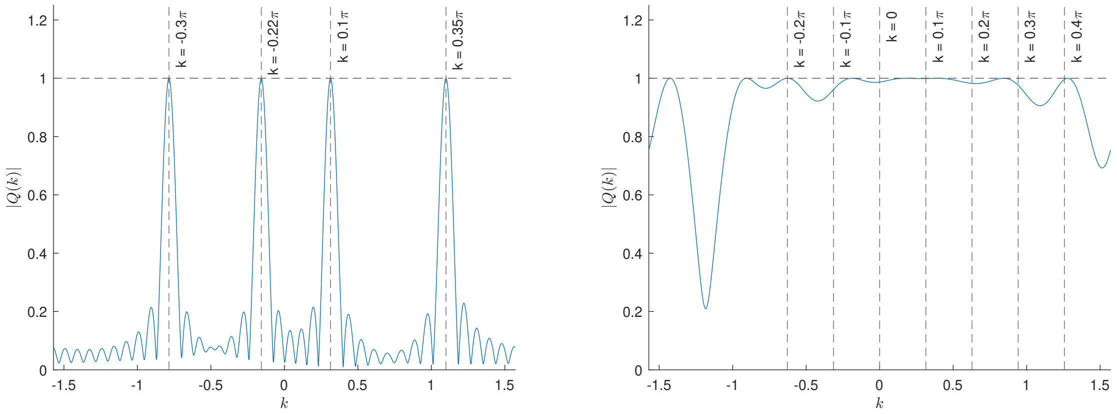

(a) Successful recovery.

(b) Unsuccessful recovery.

Figure 5.1: Magnitude of the dual polynomial for (a) successful and (b) unsuccessful recovery. The location of the actual frequencies in the signal are indicated by vertical dotted lines.

N that lay in the Nyquist range $(-\pi F, \pi F)$, thus $\hat{N} = N$. Secondly the Root Mean Squared Error (RMSE) must be smaller than $\epsilon = 10^{-5}$, thus

$$\text{RMSE} = \sqrt{\frac{1}{N}\sum_{n=1}^{N}(\hat{k}_n - k_n)^2} < \epsilon \tag{5.1}$$

where $\{\hat{k}_1, \dots, \hat{k}_N\}$ denote the retrieved modal frequencies and $\{k_1, \dots, k_N\}$ denote the actual modal frequencies present in the signal. The value 10^{-5} was chosen based on experiments. The RMSE value is typically in the order of 10^{-1} for unsuccessful recovery and 10^{-8} for successful recovery. The RMSE was taken as the error metric because it measures well how close the frequencies are and due to the quadratic relation it punishes a big error much harder than a small error, which is desired.

A number of Monte Carlo runs are performed for each value of α. The successes are averaged over these runs to get an estimate of the probability of successful recovery.

5.2. Atomic Norm without Prior Knowledge

In this section, we investigate the performance of the atomic norm as described in Chapter 3 and verify the corresponding bounds.

We look at the gridless framework in the MMV case without prior knowledge, thus solving the follwing optimization problem

$$\begin{aligned} \min_{\mathbf{W}\in\mathbb{C}^{L\times L}, \mathbf{u}\in\mathbb{C}^{M_t}, \tilde{\mathbf{P}}\in\mathbb{R}^{M_t\times L}} \quad & \mathrm{Tr}(\mathrm{Toep}(\mathbf{u})) + \mathrm{Tr}(\mathbf{W}) \\ \text{s.t.} \quad & \begin{bmatrix} \mathrm{Toep}(\mathbf{u}) & \tilde{\mathbf{P}} \\ \tilde{\mathbf{P}}^H & \mathbf{W} \end{bmatrix} \succcurlyeq 0 \\ & \tilde{\mathbf{P}}_i = \mathbf{P}_i, \quad \forall i \in \mathcal{J}_o. \end{aligned} \tag{5.2}$$

We perform the frequency separation simulation as described in Section 5.1.2 with the parameters in Table 5.1. We compare two different settings, once with $L = 3$ and once with $L = 10$. The probability of successful recovery is shown in Fig. 5.2.

From Fig. 5.2 we make the following observations:

- The derived bound in (3.19) is respected; the derived bound is necessary, but not sufficient, and thus the probability of successful recovery only reaches one at points where the bound is met.
- The atomic norm attains values close to the bound and in practice it performs better than the $\alpha = 4$ that was theoretically proven for the general case (meeting the independence assumption on the $\boldsymbol{\phi}_k$'s) by [7].

Table 5.1: Parameters used to generate Fig. 5.2.

Parameters	M_t	M_o	F	x_0
Value	15	15	3	1.432

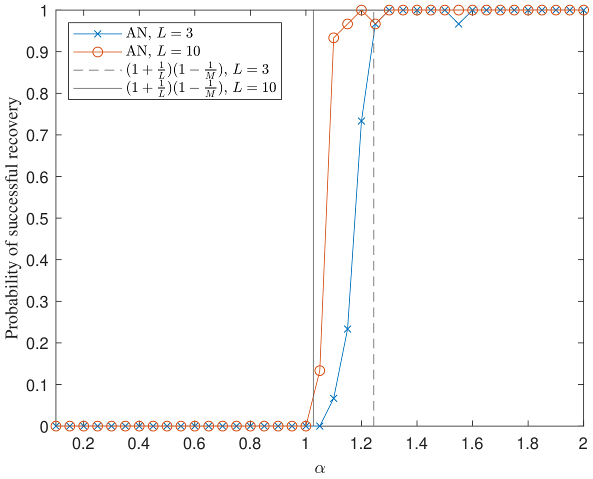

Figure 5.2: Probability of successful recovery with respect to the frequency separation for $L = 3$ and $L = 10$ excitation frequencies, averaged over 30 Monte Carlo runs.

- As suggested by the derived bound in (3.19), increasing the number of excitation frequencies L leads to a smaller lower bound on α, and the atomic norm also attains lower values if more excitation frequencies are included.
- The atomic norm is not able to reach $\alpha < 0.5$ and is thus not able to perfectly reconstruct the modal frequencies of a one-dimensional room.

5.3. Atomic Norm with Prior Knowledge

In this section, we investigate the effect of adding prior knowledge to the framework, as discussed in Chapter 4, in terms of achievable frequency separation.

5.3.1. Exploiting the Shape of the Steering Matrix

As suggested in Section 4.1 we can either shrink the solution space for the optimization parameter $\mathbf{u}$ from the complex to the real numbers or we can add an extra equality constraint on the Toeplitz matrix. This forces the (spatial) frequency spectrum to be symmetric with respect to the zero frequency. The proposed optimization problem is

$$\begin{aligned} \min_{\mathbf{W}\in\mathbb{C}^{L\times L},\mathbf{u}\in\mathbb{C}^{M_t},\tilde{\mathbf{P}}\in\mathbb{R}^{M_t\times L}} \quad & \operatorname{Tr}(\operatorname{Toep}(\mathbf{u})) + \operatorname{Tr}(\mathbf{W}) \\ \text{s.t.} \quad & \begin{bmatrix} \operatorname{Toep}(\mathbf{u}) & \tilde{\mathbf{P}} \\ \tilde{\mathbf{P}}^H & \mathbf{W} \end{bmatrix} \succcurlyeq 0 \\ & \tilde{\mathbf{P}}_i = \mathbf{P}_i, \quad \forall i \in \mathcal{J}_o \\ & \mathbf{\Pi}_M \operatorname{Toep}(\mathbf{u}) \mathbf{\Pi}_M = \operatorname{Toep}(\mathbf{u}). \end{aligned} \tag{5.3}$$

We again perform the frequency separation simulation as described in Section 5.1.2, with the parameters in Table 5.2. We compare the gridless framework with and without constraint. The probability of successful recovery is shown in Fig. 5.3.

As expected, the reconstruction is not improved by the extra constraint because the optimal solution was already inside the solution space ($\mathbb{R}^{M_t} \subset \mathbb{C}^{M_t}$). The derived bound is still respected.

5.3.2. Exploiting the Mirror Image Model

We simulate the model with a mirror image in one wall, as described in Section 4.2. The corresponding optimization problem is given by

Table 5.2: Parameters used to generate Fig. 5.3.

Parameters	M_t	M_o	F	L	x_0
Value	15	15	3	10	1.432

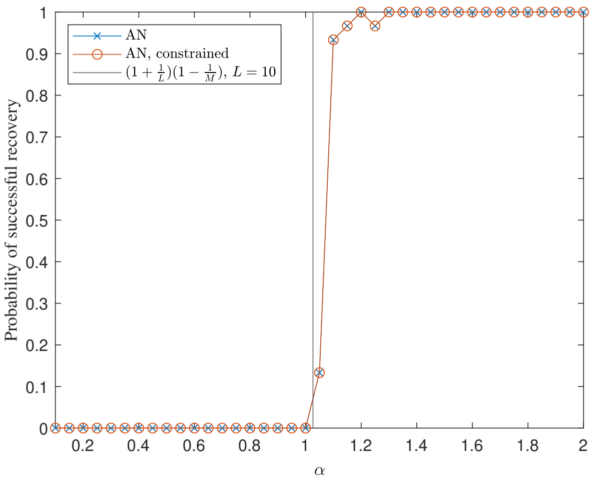

Figure 5.3: Probability of successful recovery with respect to the frequency separation, with and without constraint, averaged over 30 Monte Carlo runs.

$$\begin{aligned}
\min_{\mathbf{W}\in\mathbb{C}^{L\times L},\mathbf{u}\in\mathbb{R}^{2M_t},\tilde{\mathbf{P}}\in\mathbb{R}^{2M_t\times L}} \quad & \mathrm{Tr}(\mathrm{Toep}(\mathbf{u})) + \mathrm{Tr}(\mathbf{W}) \\
\text{s.t.} \quad & \begin{bmatrix} \mathrm{Toep}(\mathbf{u}) & \tilde{\mathbf{P}} \\ \tilde{\mathbf{P}}^H & \mathbf{W} \end{bmatrix} \succcurlyeq 0 \\
& \tilde{\mathbf{P}}_i = \begin{bmatrix} \mathbf{\Pi}_{M_t}\mathbf{P}^* \\ \mathbf{P} \end{bmatrix}_i, \forall i \in \mathcal{J}_o.
\end{aligned} \tag{5.4}$$

We perform the frequency separation simulation as described in Section 5.1.2, with the parameters in Table 5.3. We compare the framework with and without the mirror image. The probability of successful recovery is shown in Fig. 5.4. From the figure we make a few remarks. First of all, the framework including the mirror image clearly outperforms the framework without mirror image. Secondly, the framework including the mirror image reaches success below the lower bound $(1+\frac{1}{L})(1-\frac{1}{M})$, but still respects the newly derived bound of $\frac{1}{2}(1+\frac{1}{L})(1-\frac{1}{M})$.

Table 5.3: Parameters used to generate Fig. 5.4.

Parameters	M_t	M_o	F	L	x_0
Value	15	15	3	10	1.432

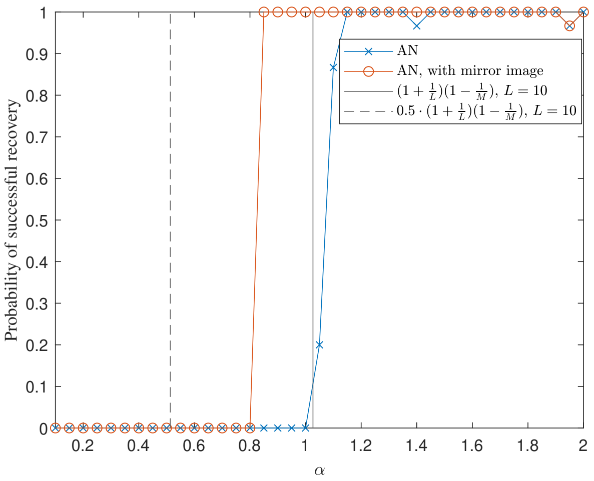

Figure 5.4: Probability of successful recovery with respect to the frequency separation, with and without mirror image, averaged over 30 Monte Carlo runs.

5.3.3. Exploiting Spectral Symmetry

Finally we also include the Hilbert transform, as described in Section 4.3. In the simulation we thus neglect the negative frequencies. The optimization problem is given by

$$\begin{aligned}
\min_{\mathbf{W}\in\mathbb{C}^{L\times L},\mathbf{u}\in\mathbb{C}^{2M_t},\tilde{\mathbf{P}}\in\mathbb{R}^{2M_t\times L}} \quad & \mathrm{Tr}(\mathrm{Toep}(\mathbf{u})) + \mathrm{Tr}(\mathbf{W}) \\
\text{s.t.} \quad & \begin{bmatrix} \mathrm{Toep}(\mathbf{u}) & \tilde{\mathbf{P}} \\ \tilde{\mathbf{P}}^H & \mathbf{W} \end{bmatrix} \succcurlyeq 0 \\
& \tilde{\mathbf{P}}_i = \begin{bmatrix} \mathbf{\Pi}_{M_t}\mathbf{P}^* \\ \mathbf{P} \end{bmatrix}_i, \forall i \in \mathcal{J}_o \\
e^{-ja}\mathbf{F}\mathrm{Toep}(\mathbf{u})\mathbf{G}^H + e^{ja}\mathbf{G}\mathrm{Toep}(\mathbf{u})\mathbf{F}^H & \\
-2\cos(b)\mathbf{G}\mathrm{Toep}(\mathbf{u})\mathbf{G}^H & \succcurlyeq 0.
\end{aligned} \tag{5.5}$$

We perform the frequency separation simulation as described in Section 5.1.2, with the parameters in Table 5.4. We compare three frameworks; one framework without prior knowledge and $L = 10$, one framework with prior knowledge and $L = 10$ and one framework with prior knowledge and $L = 50$. The probability of successful recovery is shown in Fig. 5.5.

Table 5.4: Parameters used to generate Fig. 5.5.

Parameters	M_t	M_o	F	x_0
Value	15	15	3	1.432

Parameters	a	b
Value	$\frac{\pi}{2}$	$\frac{\pi}{2}$

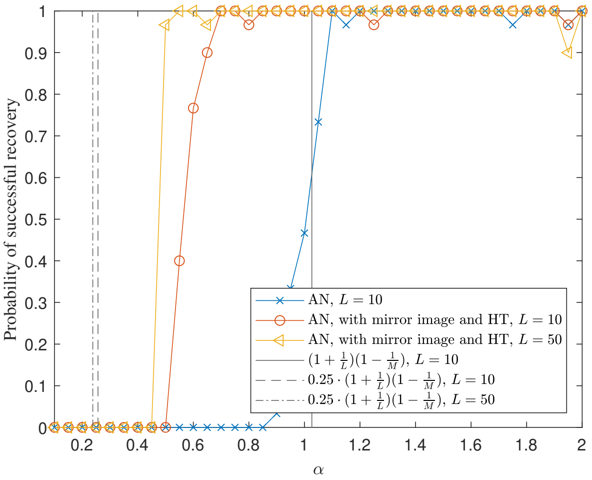

Figure 5.5: Probability of successful recovery with respect to the frequency separation, with and without prior knowledge, averaged over 30 Monte Carlo runs.

From Fig. 5.5 we conclude that if the negative frequencies are neglected and we include a mirror image, then successful recovery is reached for $\alpha = \frac{1}{2}$, provided that we use $L = 50$. This means that with this framework we are able to perfectly reconstruct the modal frequencies of the room modes.

Finally we simulate the room according to Section 3.1, with the correct modal frequencies, $k_n = n\frac{\pi}{L_x}$. We solve the optimization problem that includes all prior knowledge, i.e. Eq. (5.5). Note that only the positive frequencies are simulated, thus the first $\frac{N-1}{2}$ columns of $\mathbf{A}$ are omitted. The parameters used for the simulation are shown in Table 5.5. The magnitude of the dual polynomial of the problem is shown in Fig. 5.6. Due to the frequency restriction constraint the dual polynomial is only bounded in the allowed frequency range, $[0, \pi F)$. The dual polynomial attains one exactly at the modal frequencies, and thus perfectly reconstructs the frequencies. From the figure it can be seen that the dual polynomial still has a rather high magnitude in between its peaks. Therefore this framework will probably not be robust against interference such as noise. To increase the robustness one could add more excitation frequencies.

Table 5.5: Parameters used to generate Fig. 5.6.

Parameters	M_t	M_o	F	x_0
Value	15	15	3	1.432

Parameters	L_x	N	a	b
Value	5	29	$\frac{\pi}{2}$	$\frac{\pi}{2}$

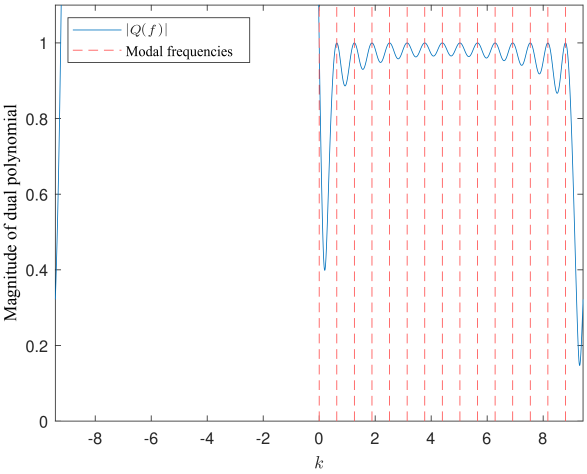

Figure 5.6: Magnitude of dual polynomial.

5.4. Summary

In this chapter we have simulated various versions of the proposed gridless framework. We list the main conclusions of this chapter:

- The bounds derived in Chapter 3 are confirmed by simulation. The gridless framework without prior knowledge is not able to reach successful recovery at the (spatial) frequency separation of the room modes.
- By including prior knowledge the framework can perform better in terms of frequency separation. We have suggested three options of which the mirror image in conjunction with the Hilbert transform results in successful recovery at the frequency separation of the room modes.

We can thus give a positive answer to the research question Eq. (RQ.1); it is possible to formulate a gridless framework for estimating room modes instead of the conventional on-the-grid method.

6

Conclusion

This master thesis has focused on formulating a gridless framework for estimating room modes for sound field reconstruction in enclosed spaces. Current on-the-grid methods for sound field reconstruction try to estimate the room modes using the ℓ_1-norm. This norm is used to promote a sparse solution from a discrete dictionary. Due to the fact that the dictionary is discrete, these methods suffer from a basis mismatch. Last decade a 'gridless' solution to this basis mismatch has been introduced, known as the atomic norm. The advantage of this approach is that it does not suffer from this basis mismatch problem. Consequently the research question was:

Is it possible to formulate a gridless framework for estimating
room modes instead of the conventional on-the-grid method? (RQ.1)

In this work, we thus investigated the use of a gridless framework for estimating room modes using atomic norm minimization, a gridless method. Due to the complexity of the problem we have considered the simplified case of a one-dimensional room with rigid walls.

The atomic norm cannot estimate frequencies which are arbitrarily close together. It needs a certain frequency separation in order to guarantee a successful recovery of the modal frequencies. We showed that we can derive two bounds for this frequency separation in the signal. One upper bound which is required by the separation of the modal frequencies or room modes, and one necessary (but not sufficient) lower bound following from the number of known variables and unknown variables. If no additional prior knowledge is added to the problem, the lower bound is larger than the upper bound, resulting in a feasibility problem. The derived bounds are verified by simulation results. This means that the spatial frequencies of room modes are too dense in the (spatial) frequency domain to meet the frequency separation required by the atomic norm for perfect reconstruction.

Because the frequency separation required by the atomic norm is not met, it computes an approximation of the signal and we can not establish performance guarantees. This means that without prior knowledge, formulating a gridless framework that can successfully recover the modal frequencies of a one-dimensional room is not possible. However, due to the bounds we derived, we get insight into how the framework should be altered if prior knowledge is available.

We looked at various methods which incorporate prior knowledge into the proposed gridless framework. We show how the derived bound can be lowered if prior knowledge is exploited. Also, we show that perfect recovery is possible in the one-dimensional setting by exploiting both the structure of the sound field and the acquisition method. Thus, including prior knowledge, formulating a gridless framework that can successfully recover the modal frequencies of a one-dimensional room is possible.

7

Future Work

In this chapter we reflect on the presented work and discuss the challenges that lie ahead. The future work is divided into the following topics; non-rigid walls, higher dimensions, computational complexity and noise.

Non-rigid walls In this work we have only considered rigid walls. However, in realistic scenarios the walls will be non-rigid. This affects the room modes; in Appendix C we show that their shape remains the same, however the corresponding modal frequencies become complex. Moreover, the modal frequencies are not easy to obtain as one needs to solve a highly non-linear equation.

The complex modal frequencies result in so-called damped room modes. This makes the scenario with non-rigid walls more complicated than its rigid counterpart. Literature has proposed different models for the non-rigid wall case. Often an approximate model is used for simplicity. The interested reader is referred to [30].

Due to the fact that the modal frequencies now have a real and a complex part, the frequency estimation problem becomes two-dimensional. If the aim is to estimate the room modes with the atomic norm in the the non-rigid wall case, a good starting point would be therefore to study [31]. It would be interesting if and how the bounds derived in this work can be extended to the non-rigid wall case.

Higher dimensions Another step towards a more realistic scenario is to include a second or even a third dimension. Although it is a very recent topic, adding dimensions to the atomic norm has been studied for some years. In [31] the two-dimensional case is vectorized such that the resulting SDP is very similar to the SMV case, although the Toeplitz matrix has more structure. This "vectorized" method can also be extended to higher dimensions. In [32] the Vandermonde decomposition is extended to multi dimensional settings. Some theoretical guarantees are given by [33]. In [34] a method was described to calculate the atom norm in higher dimensions ($D \geq 2$) via the dual problem.

We have started looking at extending our bounds for one-dimensional rooms to two or three dimensions. We can conclude that this extension is relatively straight forward, as the room modes can be decoupled into an x and a y component. However, there is some trouble verifying the bounds which is due to the fact that one has more than one dimension. Additionally, we have found that, similar to the one-dimensional case, the bounds show that the gridless framework is not able to make a successful reconstruction if no prior knowledge is added. In general we see two main challenges for higher dimensions.

First of all, the effect of the moving microphone can not be extended to higher dimensions easily. Instead of measuring continuously on a line, one would need to measure continuously on a area or in a volume, which is not possible. Thus, other approaches need to be invented in order to be able to apply the continuous Hilbert transform.

Secondly, the computational complexity of the atomic norm increases drastically with the number of dimensions. This could pose a problem in real time scenarios. In [35] a so called "decoupled" form of the atomic norm is proposed, which reduced the computational time significantly with respect to the method proposed by [31]. However, the decoupled atomic norm is only defined for the two-dimensional setting. It is still an open problem to define a decoupled framework for three dimensions or more.

Computational complexity Throughout this work we have not considered the computational complexity of the gridless framework or compared it to the on-the-grid methods. This has a couple of reasons. First of all, in this work we have considered exciting the room with a source, and thus implicitly assume that there is enough time to first ”measure” the room. In such a setting, the complexity or time to solve the problem is not of first priority. Secondly, the computational complexity in one dimension is not representative for realistic scenarios. Comparing is thus not very insightful.

Computational complexity becomes important when we turn to a dynamic scenario, for example if the objects in the room change position over time. Since the geometry and the objects inside the room affect the shape and frequencies of the room modes, one would need to continuously estimate the room modes to be able to reconstruct the sound field.

Additionally, we want to stress that if more dimensions are added to the gridless framework, the computational complexity will generally start to grow exponentially. Several studies have investigated strategies to compute the atomic norm such that the computational complexity increases linearly with the number of dimensions (see e.g. [35, 36, 37]).

Robustness In this work we have only considered a signal model without additive noise convolutive noise or an error source, because this allows to derive deterministic bounds. However, the gridless framework can be adapted to include any type of disturbances. For example, to include additive (Gaussian) noise, the equality constraint would have to be changed into an inequality constraint. A Frobenius norm could be used to minimize the noise power in the solution. Note that due to the presence of the noise, the solution of the gridless framework will not be exact anymore.

However, as mentioned, additive noise would not have to be the only disturbance. We have not investigated the possible origins of disturbances. Moreover, the distribution of the noise was not studied but is important as it might affect the way in which the optimization problem has to be adapted.

Bibliography

[1] M. Olik, J. Francombe, P. Coleman, P. Jackson, M. Olsen, M. Møller, R. Mason, and S. Bech, “A comparative performance study of sound zoning methods in a reflective environment,” in *Proceedings of the AES International Conference*, Sep. 2013.

[2] J. Cheer and S. Elliott, “Design and implementation of a personal audio system in a car cabin,” *The Journal of the Acoustical Society of America*, vol. 133, pp. 3251–3260, May 2013.

[3] T. Betlehem, W. Zhang, M. Poletti, and T. Abhayapala, “Personal sound zones: Delivering interface-free audio to multiple listeners,” *IEEE Signal Processing Magazine*, vol. 32, no. 2, pp. 81–91, 2015.

[4] S. Verburg and E. Fernandez-Grande, “Reconstruction of the sound field in a room using compressive sensing,” *The Journal of the Acoustical Society of America*, vol. 143, pp. 3770–3779, Jun. 2018.

[5] E. Fernandez-Grande, “Sound field reconstruction in a room from spatially distributed measurements,” in *Proceedings of the 23rd International Congress on Acoustics*, pp. 4961–4968, 2019.

[6] T. Pham Vu and H. Lissek, “Low frequency sound field reconstruction in a non-rectangular room using a small number of microphones,” *Acta Acustica*, vol. 4, pp. 1–14, 2020.

[7] G. Tang, B. Bhaskar, P. Shah, and B. Recht, “Compressed sensing off the grid,” *IEEE Transactions on Information Theory*, vol. 59, no. 11, pp. 7465–7490, 2013.

[8] E. Candès and C. Fernandez-Granda, “Towards a mathematical theory of super-resolution,” *Communications on Pure and Applied Mathematics*, vol. 67, Jun. 2014.

[9] S. Cecchi, A. Carini, and S. Spors, “Room response equalization - a review,” *Applied Sciences*, vol. 8, no. 1, 2018. Art. no. 16.

[10] P. A. Naylor and N. D. Gaubitch, *Speech Dereverberation.* Springer, 2010.

[11] F. Lluís, P. Martínez-Nuevo, M. Møller, and S. E. Shepstone, “Sound field reconstruction in rooms: inpainting meets super-resolution,” *The Journal of the Acoustical Society of America*, vol. 148, pp. 649–659, Aug. 2020.

[12] E. G. Williams, *Fourier Acoustics: Sound Radiation and Nearfield Acoustical Holography.* Academic Press, 1999.

[13] H. Kuttruff, *Room acoustics.* Spon Press, 4th ed., 2005.

[14] R. de Prony, “Essai experimentale et analytique,” *Journal de l’Ecole Polytechnique Floréal et Plairial*, vol. 1, pp. 24–76, 1795.

[15] A. Paulraj, R. Roy, and T. Kailath, “Estimation of signal parameters via rotational invariance techniques- esprit,” in *Nineteeth Asilomar Conference on Circuits, Systems and Computers, 1985.*, pp. 83–89, 1985.

[16] R. Roy and T. Kailath, “Esprit-estimation of signal parameters via rotational invariance techniques,” *IEEE Transactions on Acoustics, Speech, and Signal Processing*, vol. 37, no. 7, pp. 984–995, 1989.

[17] R. Schmidt, “Multiple emitter location and signal parameter estimation,” *IEEE Transactions on Antennas and Propagation*, vol. 34, no. 3, pp. 276–280, 1986.

[18] R. Tibshirani, “Regression shrinkage and selection via the lasso,” *Journal of the Royal Statistical Society. Series B (Methodological)*, vol. 58, no. 1, pp. 267–288, 1996.

[19] D. Donoho, “Compressed sensing,” *IEEE Transactions on Information Theory*, vol. 52, no. 4, pp. 1289–1306, 2006.

[20] E. J. Candes and M. B. Wakin, “An introduction to compressive sampling,” *IEEE Signal Processing Magazine*, vol. 25, no. 2, pp. 21–30, 2008.

[21] S. Boyd and L. Vandenberghe, *Convex Optimization.* Cambridge University Press, 2004.

[22] Y. Chi, L. Scharf, A. Pezeshki, and A. Calderbank, “Sensitivity to basis mismatch in compressed sensing,” *IEEE Transactions on Signal Processing*, vol. 59, no. 5, pp. 2182–2195, 2011.

[23] C. Fernandez-Granda, “Super-resolution of point sources via convex programming,” in *2015 IEEE 6th International Workshop on Computational Advances in Multi-Sensor Adaptive Processing (CAMSAP)*, pp. 41–44, 2015.

[24] Z. Yang and L. Xie, “Exact joint sparse frequency recovery via optimization methods,” *IEEE Transactions on Signal Processing*, vol. 64, no. 19, pp. 5145–5157, 2016.

[25] J. Allen and D. Berkley, “Image method for efficiently simulating small room acoustics,,” *The Journal of the Acoustical Society of America*, vol. 65, pp. 943–950, Apr. 1979.

[26] R. N. Bracewell, “Relatives of the fourier transform,” in *The Fourier Transform And Its Aplications*, ch. 13, McGraw-Hill, 3rd ed., 1999.

[27] J. Unnikrishnan and M. Vetterli, “Sampling and reconstruction of spatial fields using mobile sensors,” *IEEE Transactions on Signal Processing*, vol. 61, no. 9, pp. 2328–2340, 2013.

[28] T. Ajdler, L. Sbaiz, and M. Vetterli, “Dynamic measurement of room impulse responses using a moving microphone,” *The Journal of the Acoustical Society of America*, vol. 122, no. 3, pp. 1636–1645, 2007.

[29] H.-H. Chao and L. Vandenberghe, “Extensions of semidefinite programming methods for atomic decomposition,” in *2016 IEEE International Conference on Acoustics, Speech and Signal Processing (ICASSP)*, pp. 4757–4761, 2016.

[30] P. A. Nelson and S. J. Elliot, “Global control of enclosed sound fields,” in *Active Control of Sound*, ch. 10, Academic Press, 1st ed., 1992.

[31] Y. Chi and Y. Chen, “Compressive two-dimensional harmonic retrieval via atomic norm minimization,” *IEEE Transactions on Signal Processing*, vol. 63, no. 4, pp. 1030–1042, 2015.

[32] Z. Yang, L. Xie, and P. Stoica, “Vandermonde decomposition of multilevel toeplitz matrices with application to multidimensional super-resolution,” *IEEE Transactions on Information Theory*, vol. 62, no. 6, pp. 3685–3701, 2016.

[33] I. Valiulahi, S. Daei, F. Haddadi, and F. Parvaresh, “Two-dimensional super-resolution via convex relaxation,” *IEEE Transactions on Signal Processing*, vol. 67, no. 13, pp. 3372–3382, 2019.

[34] W. Xu, J.-F. Cai, K. V. Mishra, M. Cho, and A. Kruger, “Precise semidefinite programming formulation of atomic norm minimization for recovering d-dimensional (d$\geq$2) off-the-grid frequencies,” in *2014 Information Theory and Applications Workshop (ITA)*, pp. 1–4, 2014.

[35] Z. Tian, Z. Zhang, and Y. Wang, “Low-complexity optimization for two-dimensional direction-of-arrival estimation via decoupled atomic norm minimization,” in *2017 IEEE International Conference on Acoustics, Speech and Signal Processing (ICASSP)*, pp. 3071–3075, 2017.

[36] X. Wu, W. Zhu, and J. Yan, “A fast gridless covariance matrix reconstruction method for one- and two-dimensional direction-of-arrival estimation,” *IEEE Sensors Journal*, vol. 17, no. 15, pp. 4916–4927, 2017.

[37] Y. Zhang, Y. Wang, Z. Tian, G. Leus, and G. Zhang, “Low-complexity gridless 2d harmonic retrieval via decoupled-anm covariance reconstruction,” in *2020 28th European Signal Processing Conference (EUSIPCO)*, pp. 1876–1880, 2021.

[38] Y. Naka, A. Oberai, and B. Shinn-Cunningham, “Acoustic eigenvalues of rectangular rooms with arbitrary wall impedances using the interval newton/generalized bisection method,” *The Journal of the Acoustical Society of America*, vol. 118, pp. 3662–3671, Dec. 2005.

[39] P. M. Morse and R. H. Bolt, “Sound waves in rooms,” *Reviews of Modern Physics*, vol. 16, pp. 69–150, Apr. 1944.

[40] S. Bistafa and J. Morrissey, “Numerical solutions of the acoustic eigenvalue equation in the rectangular room with arbitrary (uniform) wall impedances,” *Journal of Sound and Vibration*, vol. 263, pp. 205–218, May 2003.

A

EUSIPCO Paper

On March 1st (2022) the conference paper as shown on the following pages was submitted to the Europian Signal Processing Conference (EUSIPCO) 2022 as a part of the special session "Hearing the Walls: Methods and Applications for the Interference of Geometric and Acoustic Properties of Reverberant Environments". At the moment of writing this thesis it was yet unknown if the submitted paper was accepted.

Towards Gridless Sound Field Reconstruction

Ids van der Werf*†, Pablo Martínez-Nuevo*, Martin Møller*, Richard Hendriks† and Jorge Martínez†
*Bang & Olufsen, †Delft University of Technology

***Abstract*—The sound field in a room can be represented by a weighted sum of room modes. To estimate the room modes, current literature uses on-the-grid, sparse reconstruction methods. However, these on-the-grid methods are known to suffer from basis mismatch. In this work, we investigate the use of a gridless framework for estimating room modes using atomic norm minimization, a gridless method. The advantage of this approach would be that it does not suffer from this basis mismatch problem. We derive a bound for the sound field reconstruction problem in a one-dimensional room with rigid walls and relate this to the frequency separation that is required by the atomic norm. We conclude that for perfect reconstruction based on the investigated gridless approach, additional prior knowledge about the signal model is required. We show how recovery is possible in a one-dimensional setting by exploiting the structure of the sound field and the acquisition method.**

***Index Terms*—atomic norm, sparse recovery, (spatial) frequency estimation, room acoustics, sound field reconstruction**

I. INTRODUCTION

Knowing how the sound pressure varies over space and time has many applications, e.g., room compensation [1], dereverberation [2], and sound zone reconstruction [3]. Reconstructing sound fields inside enclosures come with extra challenges as the surroundings, such as the geometry of the enclosure and the materials used, influence the sound field. Reconstructing a satisfying sound field in the whole enclosure by extrapolating from few measurements is thus not an obvious task.

For ease of illustration, we focus on rectangular rooms in this paper (see Fig. 1). However, the principles here can be extended to any enclosure. Typically, microphones, indicated in Fig. 1 by the red dots, are used to measure the sound pressure. However, the microphones cannot be placed arbitrarily across the room, but are typically placed upon the physical objects inside the room. This means that in practice only a small number of microphones can be used. From the sound pressure measured at the microphone locations, the sound pressure in the whole room must be estimated, as shown in the lower half of Fig. 1.

Several solutions for sound field reconstruction have been proposed in the past, e.g. [4]–[7]. Assuming that the room modes can be expanded into plane waves, current literature estimates the corresponding modal frequencies [5]–[7]. Knowledge about the shape of the room modes and the modal frequencies of a room is very useful, as it allows to calculate the sound field resulting from any source receiver pair.

In the low frequency range, the sound field can be represented by a small number of room modes. Therefore, estimating room modes is done by the use of compressive sensing techniques and convex optimization (e.g. [6], [7]), due to its versatility to include prior knowledge about the setting. These approaches use methods based on the lasso problem [8], which use a sparsity promoting ℓ_1-norm. Such methods are often referred to as 'on-the-grid' methods, as they use a grid to form a basis. However, they suffer from what is called basis mismatch [9] [10], because the assumed basis never exactly matches the actual basis of the signal. As a result on-the-grid methods will always make an approximation of the room modes, and will never produce an exact reconstruction.

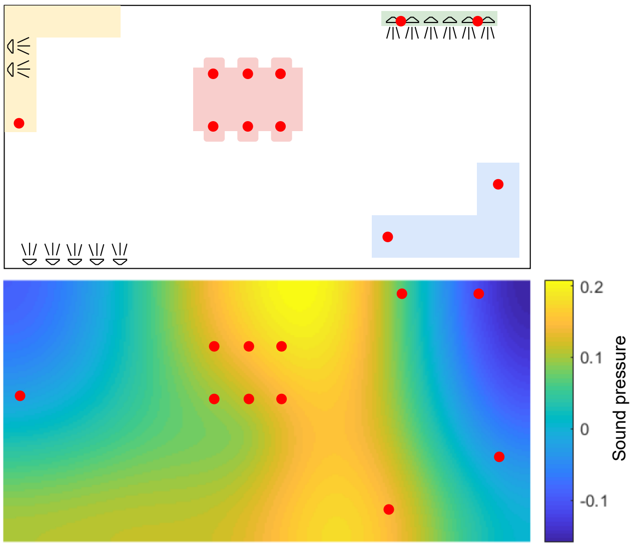

Fig. 1. Living room and corresponding sound field at 150 Hz

Last decade a 'gridless' solution to this basis mismatch has been introduced, known as the atomic norm [11], [12]. In this work we investigate whether a gridless framework using the atomic norm can be used as a replacement for the on-the-grid methods for the estimation of modal frequencies. We start by studying a model of a room that has been simplified significantly, in order to reduce the complexity of the problem. However, its analysis gives insights into the challenges ahead, even for more complicated scenarios.

The remainder of this paper is organized as follows. First, in Section II, the signal model is introduced, as well as the on-the-grid and proposed gridless approach. Then in Section III we derive a theoretical bound for the sound field reconstruction problem in a boxed-shaped room and compare this with the frequency separation required by the atomic norm for a successful signal recovery. In Section IV we discuss how to include prior knowledge about the signal model and exploit the acquisition method, finally we validate the derived bound with numerical simulations in Section V.

II. MODAL FREQUENCY ESTIMATION

A. Signal Model

For simplicity and without loss of generality we will look at a one dimensional room with rigid walls.We assume that the room has length L_x and is excited by a point source located at $x = x_0$. The Green's function in this setting is defined as

$$G(x, x_0, \omega) = -\frac{1}{L_x} \sum_{n=0}^{\infty} \frac{\psi_n(x_0)}{(\frac{\omega}{c})^2 - k_n^2} \psi_n(x), \tag{1}$$

where c is the speed of sound and $\psi_n(x)$ is the n'th room mode (eigenfunction) with corresponding n'th modal frequency k_n (eigenfrequency). Let us assume the source emits L temporal frequencies indicated by ω_l. The sound field is then defined as

$$p(x, \omega) = -\frac{1}{L_x} \sum_{l=1}^{L} C_l \delta(\omega - \omega_l) \sum_{n=0}^{\infty} \frac{\psi_n(x_0)}{(\frac{\omega}{c})^2 - k_n^2} \psi_n(x), \tag{2}$$

where $C_l \in \mathbb{R}$ is a constant, which allows for excitation frequencies with varying amplitudes. For a room with rigid walls, $\psi_n(x) = \sqrt{2} \cos(k_n x)$ and $k_n = n \frac{\pi}{L_x}$ [13].

In total, we define M_t potential microphone positions inside the room on a uniform grid, i.e., $x_m = \frac{m}{F}$ where $m \in \mathcal{J}_t$ for $\mathcal{J}_t = \{1, 2, \ldots, M_t\}$ and $\frac{1}{F}$ is the distance between successive positions. Note that $x_m \in (0, L_x)$. Similarly, we denote by $\mathcal{J}_o$ the subset of indexes corresponding to the observed measurements, i.e., $\mathcal{J}_o \subseteq \mathcal{J}_t$. We place $M_o \leq M_t$ microphones at positions chosen uniformly at random from the index set $\mathcal{J}_t$, to form the 'observed' set. The situation is illustrated in Fig. 2.

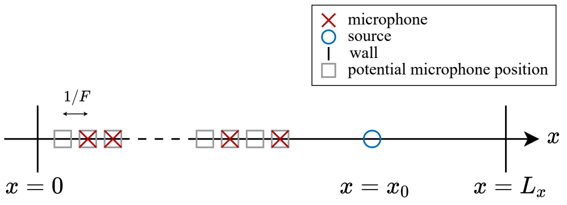

Fig. 2. Measurement setup in a 1D room

Using the complex exponential expansion for the cosine function, and assuming we can satisfyingly represent the sound field with a finite number of N room modes, we can define a system of equations over the set $\mathcal{J}_t$ as

$$\mathbf{P} = \mathbf{A}\mathbf{S}, \tag{3}$$

where the potential measurements are stacked in the matrix $\mathbf{P} \in \mathbb{R}^{M_t \times L}$, with columns $\mathbf{p}_l = [p(x_1, \omega_l), \ldots, p(x_{M_t}, \omega_l)]^T$, $\mathbf{A} = [\mathbf{a}(k_1), \ldots, \mathbf{a}(k_N)] \in \mathbb{C}^{M_t \times N}$ is the steering matrix containing the set of modal frequencies, $\mathbf{a}(k_n) = [e^{jk_n x_1}, e^{jk_n x_2}, \ldots]^T$, with $n \in \{-\frac{N-1}{2}, \ldots, +\frac{N-1}{2}\}$, $\mathbf{S} \in \mathbb{C}^{N \times L}$ is the source matrix containing the weights of each modal frequency, with elements $s_{n,l} = -\frac{C_l}{L_x} \frac{\cos(k_n x_0)}{(\frac{\omega_l}{c})^2 - k_n^2}$. In general this system is underdetermined, $N > M_t$. However, the columns of the source matrix are approximately sparse, as only the room modes with modal frequencies close to $\frac{\omega_l}{c}$ get excited significantly. This allows for compressive sensing techniques to solve the problem.

B. Existing On-the-grid Method

In order to determine the modal frequencies and corresponding amplitudes, prior art (e.g. [6], [7]) minimizes an ℓ_1-norm of a weighted (sparse) vector $\mathbf{b}_l$,

$$\begin{aligned} \min_{[\mathbf{b}_1, \mathbf{b}_2, \ldots, \mathbf{b}_L] \in \mathbb{C}^{R \times L}} \quad & \textstyle\sum_l^L ||\mathbf{L}_l \mathbf{b}_l||_1 \\ \text{s.t.} \quad & \mathbf{P}_i - \mathbf{D}[\mathbf{b}_1, \mathbf{b}_2, \ldots, \mathbf{b}_L] = 0, \forall i \in \mathcal{J}_o \end{aligned} \tag{4}$$

where the basis $\mathbf{D}$ is formed by a dictionary of R spatial frequencies $v_r \in [-\pi F, \pi F]$ on a uniform grid and weighting $\mathbf{L}_l = \text{diag}((\frac{\omega_l}{c})^2 - \mathbf{v}^2)$, $\mathbf{v} = [v_1, \ldots, v_R]^T$.

The basis mismatch problem results from the discrete dictionary $\mathbf{D}$. One assumes that the modal frequencies are inside this dictionary, but in practice this is never exactly the case resulting in a mismatch between the actual basis $\mathbf{A}$ and the assumed basis $\mathbf{D}$. If the size of the dictionary is increased, the mismatch decreases, however this comes with computational costs and higher coherence between the columns of $\mathbf{D}$ [14]. If the dictionary is too small, the modal frequencies might not be in the dictionary, decreasing the accuracy of the reconstruction. If an on-the-grid method is used, one thus has to tackle this trade-off and will inherently make an error due to the fact that a grid is used.

C. Proposed Method

To circumvent the basis mismatch problem we investigate the use of a gridless framework, using the atomic norm. This method makes use of a set of atoms as dictionary,

$$\mathcal{A} = \{\mathbf{a}(f, \boldsymbol{\phi}) = \mathbf{a}(f)\boldsymbol{\phi} \, : f \in [0, F), \boldsymbol{\phi} \in \mathbb{C}^{1 \times L}, ||\boldsymbol{\phi}||_2 = 1\}, \tag{5}$$

where $\mathbf{a}(f) = [e^{j2\pi f x_1}, \ldots, e^{j2\pi f x_{M_t}}]^T \in \mathbb{C}^{M_t}$. Note that the frequency f is defined over a continuous interval, therefore the set defines a continuous dictionary. The atomic (ℓ_1) norm is defined as

$$||\mathbf{P}||_{\mathcal{A}} = \inf \left\{ \sum_{k \in \mathcal{K}} c_k : \mathbf{P} = \sum_{k \in \mathcal{K}} c_k \mathbf{a}(f_k, \boldsymbol{\phi}_k), \mathbf{a}(f_k, \boldsymbol{\phi}_k) \in \mathcal{A} \right\}, \tag{6}$$

where $c_k > 0$ and $\mathcal{K}$ is the set containing the indices of the atoms. Alternatively to (4), we use the atomic norm to promote a sparse set of modal frequencies:

$$\min_{\tilde{\mathbf{P}} \in \mathbb{C}^{M_t \times L}} ||\tilde{\mathbf{P}}||_{\mathcal{A}}, \text{ s.t. } \tilde{\mathbf{P}}_i = \mathbf{P}_i, \quad \forall i \in \mathcal{J}_o, \tag{7}$$

here $\mathbf{P}_i$ denotes the i'th row of $\mathbf{P}$. The atomic norm can be cast into an SDP [12]. Therefore the optimization problem is reformulated as

$$\begin{aligned} \min_{\mathbf{W}\in\mathbb{C}^{L\times L},\mathbf{u}\in\mathbb{C}^{M_t},\tilde{\mathbf{P}}\in\mathbb{R}^{M_t\times L}} \quad & \mathrm{Tr}(\mathrm{Toep}(\mathbf{u})) + \mathrm{Tr}(\mathbf{W}) \\ \text{s.t.} \quad & \begin{bmatrix} \mathrm{Toep}(\mathbf{u}) & \tilde{\mathbf{P}} \\ \tilde{\mathbf{P}}^H & \mathbf{W} \end{bmatrix} \succcurlyeq 0 \\ & \tilde{\mathbf{P}}_i = \mathbf{P}_i, \quad \forall i \in \mathcal{J}_o. \end{aligned} \tag{8}$$

Using the matrix $\mathrm{Toep}(\mathbf{u})$, the atomic norm tries to find a matrix related to the covariance matrix of $\mathbf{P}$. From the optimal solution $\mathrm{Toep}(\mathbf{u}^*)$, we can therefore retrieve the estimated frequencies using any subspace method. Assume that the $\boldsymbol{\phi}_k$'s are independent random variables with $\mathbb{E}[\boldsymbol{\phi}_k] = \mathbf{0}$. Then, if the modal frequencies k_n adhere to a certain frequency separation,

$$\Delta_k \geq 2\pi F \frac{\alpha}{M_t - 1}, \tag{9}$$

there exist a numerical constant C, such that

$$M_o \geq C \max\left\{ \log^2 \frac{M_t\sqrt{L}}{\delta}, N \log\frac{N}{\delta} \log\frac{M_t\sqrt{L}}{\delta} \right\}. \tag{10}$$

is sufficient to guarantee that, with probability at least $1-\delta$, the atomic norm will exactly recover the original signal [12]. Tang *et al.* [12] proved that successful recovery of the (modal) frequencies is guaranteed if α equals 4 in (9). However in practice its value can be lower [15], and depends on the parameters of the model. Note that our model only approximately meets all the assumptions on $\boldsymbol{\phi}_k$, as the rows of $\mathbf{S}$ are not completely independent. It is therefore of great interest to look at the performance of the atomic norm for our signal model, and to derive corresponding bounds on the value of α.

III. BOUNDS FOR SOUND FIELD RECONSTRUCTION

A. Frequency Separation of Modal Frequencies

The modal frequencies are given by $k_n = n\frac{\pi}{L_x}$, and thus are separated by $\Delta_k = \frac{\pi}{L_x}$. Using this, we can rewrite (9) and derive that we need at least

$$\begin{aligned} M_t &\geq 2\pi F \frac{\alpha}{\Delta_k} + 1 \\ &= 2 \cdot F \cdot \alpha \cdot L_x + 1. \end{aligned} \tag{11}$$

Additionally, the size of the room puts a limit to the number of possible measurement locations M_t; the measurements must be inside the room, thus $0 < x_m < L_x, \forall m \in \mathcal{J}_t$. From this we must have that $\min_m(x_m) = \frac{1}{F} > 0$, which is satisfied, and that

$$\max_m(x_m) = \frac{M_t}{F} < L_x, \tag{12}$$

and thus

$$M_t < F \cdot L_x. \tag{13}$$

Now we combine (11) and (13), to write

$$F \cdot \alpha \cdot 2L_x + 1 < F \cdot L_x. \tag{14}$$

The inequality in (14) will be satisfied for practical situations ($L_x > 0, F > 0$) if and only if $\alpha < \frac{1}{2}$.

In conclusion, the frequency separation required by the atomic norm, shown in (9), has to reach at least $\alpha < \frac{1}{2}$, in order to be able to solve the modal frequency estimation problem exactly. Now, before we look at the performance of the atomic norm in practice, we first derive a lower bound that is inherent to the problem itself.

B. Knowns vs. Unknowns

Due to the fact that only finite number of measurements are available in practice, the estimated modal frequencies can not be arbitrarily close. We are interested in a lower bound on the frequency separation, regardless of the method one is using to solve the problem. We can then relate this bound to the frequency separation required by the atomic norm, to get an idea of the performance of the atomic norm.

From (3) we know that we have ML knowns, the number of (real) elements from the measurement matrix $\mathbf{P}$. On the contrary, the steering matrix $\mathbf{A}$ and the source matrix $\mathbf{S}$ are unknown, resulting in $N(1+L)$ unknowns in total; N unknown frequencies in $\mathbf{A}$ (not MN because the structure of $\mathbf{A}$ is assumed to be known), and NL unknowns from $\mathbf{S}$ (of which the structure is not known). If no other prior knowledge is available, the number of unknown variables cannot be lower than the number of known ones. From this it follows that,

$$ML \geq N(1+L), \tag{15}$$

and thus,

$$\frac{1}{N} \geq \frac{(1+L)}{ML}. \tag{16}$$

Note that if N (spatial) frequencies are to be fit uniformly on a interval of length $2\pi F$, then the maximum frequency separation that can be reached is $\frac{2\pi F}{N}$, thus $\frac{2\pi F}{N} = 2\pi F \frac{\alpha}{M-1}$. As a result, and using (16),

$$\begin{aligned} \alpha = (M-1)\frac{1}{N} &\geq (M-1)\frac{(1+L)}{ML} \\ &= (1+\frac{1}{L})(1-\frac{1}{M}). \end{aligned} \tag{17}$$

From (17) it is clear that α can never be lower than $\frac{1}{2}$ provided that $L > 0$ and $N > 0$. Thus, we can conclude that the frequency separation required by the atomic norm can not be reached, by construction of the problem. This means that more prior knowledge about the problem has to be included to lower the bound derived in (17).

IV. EXPLOITING PRIOR KNOWLEDGE

We have shown that atomic norm minimization without further exploiting the structure of the problem is not enough for recovery. Thus, we need to incorporate more prior knowledge to meet the bound. In particular, we describe here two strategies used in conjunction to realize successful recovery.

A. Mirror Image

In the case of rigid walls, the sound field is perfectly reflected by the walls. Therefore we can create ”image microphones” on the other side of a wall, as illustrated in Fig. 3. For this operation, the location of the corresponding wall must be known. In order to avoid a trivial case, we assume the length of the room is not fully known, i.e., we only take as reference one of the walls and use it to duplicate the measurements by mirroring them. By including one reflection, the number of knowns is increased by a factor two, therefore the lower bound on α becomes

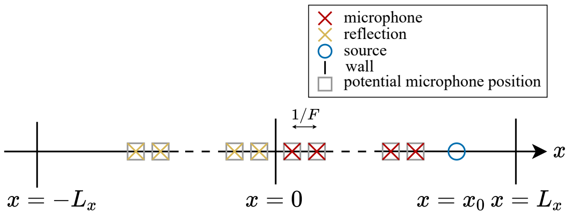

Fig. 3. 1D room with one reflection

$$\alpha \geq \frac{1}{2}(1+\frac{1}{L})(1-\frac{1}{M}). \tag{18}$$

By adding these new measurements, we have managed to reduce the constraint on the number of measurements. However, we still need to further exploit the structure of the problem to meet the inequality in (14).

B. Spectral symmetry

For the rigid wall case, the room modes are cosines. All positive modal frequencies will also occur on the negative side of the spatial frequency spectrum. Hence, we only need to consider the positive side of the spectrum. To reduce the number of unknowns, we would thus like to remove the negative side of the spectrum in our signal. This can be done by using the Hilbert transform, if a continuous measurement is available. Instead of a static grid of microphones, one could use a moving microphone, (the variable x in the signal model in (2) is replaced by vt, where v is the speed of the microphone), to get a continuous measurement in time. We assume that the Doppler effect, due to the moving microphone, can be removed [16].

First, the Hilbert transform is applied to the continuous signal, then the signal is discretized again, by $t_m = \frac{1}{v}x_m$, such that the notation is consistent. By performing the Hilbert transform, the number of unknowns is decreased by a factor two, therefore the lower bound on α becomes

$$\alpha \geq \frac{1}{4}(1+\frac{1}{L})(1-\frac{1}{M}). \tag{19}$$

Now the lower bound is smaller than $\frac{1}{2}$. Hence, the only question is whether the atomic norm attains a value lower than $\frac{1}{2}$ in practice. To ensure the framework finds a solution consisting of only positive frequencies, an extra constrained is added to the minimization problem, inspired by [17].

Assuming the negative frequencies are removed, the optimization problem becomes

$$\begin{aligned}
\min_{\mathbf{W}\in\mathbb{C}^{L\times L},\mathbf{u}\in\mathbb{C}^{2M_t},\tilde{\mathbf{P}}\in\mathbb{R}^{2M_t\times L}} \quad & \mathrm{Tr}(\mathrm{Toep}(\mathbf{u}))+\mathrm{Tr}(\mathbf{W}) \\
\text{s.t.} \quad & \begin{bmatrix}\mathrm{Toep}(\mathbf{u}) & \tilde{\mathbf{P}} \\ \tilde{\mathbf{P}}^H & \mathbf{W}\end{bmatrix} \succcurlyeq 0 \\
& \tilde{\mathbf{P}}_i = \begin{bmatrix}\mathbf{\Pi}_{M_t}\mathbf{P}^* \\ \mathbf{P}\end{bmatrix}_i, \forall i \in \mathcal{J}_o \\
e^{-ja}\mathbf{F}\mathrm{Toep}(\mathbf{u})\mathbf{G}^H + e^{ja}\mathbf{G}\mathrm{Toep}(\mathbf{u})\mathbf{F}^H & \\
-2\cos(b)\mathbf{G}\mathrm{Toep}(\mathbf{u})\mathbf{G}^H \succcurlyeq 0. &
\end{aligned} \tag{20}$$

Here $\mathbf{\Pi}_{M_t}$ is a permutation matrix with ones on its anti-diagonal, and zeros elsewhere, $a = b = \frac{\pi}{2}$ and

$$\mathbf{F} = \begin{bmatrix}\mathbf{0}_{(M_t-1),1} & \mathbf{I}_{M_t-1}\end{bmatrix}, \tag{21}$$

$$\mathbf{G} = \begin{bmatrix}\mathbf{I}_{M_t-1} & \mathbf{0}_{(M_t-1),1}\end{bmatrix}. \tag{22}$$

Note the slight abuse of notation in (20), as the index i indicates two rows, due to the reflection.

V. NUMERICAL SIMULATIONS

In Section II we mentioned that in practice $\alpha < 4$. In Section III we showed that α should be lower than $\frac{1}{2}$ for perfect signal recovery, while a lower bound is given by (17). In this section we verify the bounds with numerical simulations and show what happens if prior knowledge is included, as described in Section IV.

First, we look at the value α that is attained in practice when no prior knowledge is included. We investigate the probability of successful recovery with respect to the frequency separation as a function of α that is required by the atomic norm (see (9)). We simulate the model described by (3), however, we change the set of modal frequencies to $k_n = 2\pi F\frac{\alpha}{M_t-1}$. We consider the full data case, $M_o = M_t = 15$. The source emits L frequencies, which are i.i.d. from $\mathcal{U}[0, c\pi F)$. The modal frequency separation is changed by using different $\alpha \in \{0.5, 0.55, 0.60, \ldots, 2\}$. We solve the SDP in (8) and retrieve the frequencies by performing ESPRIT [18] on the the optimal Toeplitz matrix.

We say the signal is recovered with success if the number of retrieved modal frequencies $\hat{N}$ is equal to the actual number of modal frequencies in the signal N that lay in the Nyquist range $(-\pi F, \pi F)$, thus $\hat{N} = N$ and if additionally

$$\mathrm{RMSE} = \sqrt{\frac{1}{N}\sum_{n=1}^{N}(\hat{k}_n - k_n)^2} < 10^{-5} \tag{23}$$

where $\{\hat{k}_1, \ldots, \hat{k}_N\}$ denote the retrieved modal frequencies and $\{k_1, \ldots, k_N\}$ denote the actual modal frequencies present in the signal. In total 30 Monte Carlo runs are performed for each value of α. The successes are averaged over the runs to get an estimate of the probability of successful recovery. The result is shown in Fig. 4. We make the following observations:

- The bound derived in (17) is respected.

- The atomic norm attains values close to the bound and in practice it performs better than the $\alpha = 4$ that was theoretically proven for the general case (meeting the independence assumption on the ϕ_k's) by [12].
- As suggested by the derived bound in (17), increasing the number of excitation frequencies L leads to a smaller lower bound on α, and the atomic norm also attains lower values if more excitation frequencies are included.
- The atomic norm is not able to reach $\alpha < 0.5$ and is thus not able to perfectly reconstruct the modal frequencies of a boxed-shaped room.

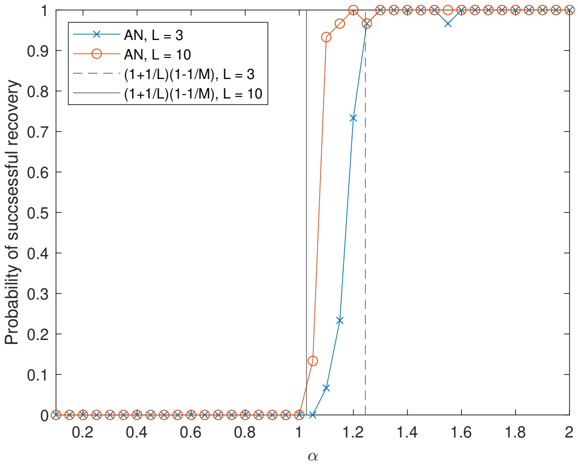

Fig. 4. Probability of successful recovery for varying frequency separation, averaged over 30 Monte Carlo runs, $M = M_o = M_t = 15$

Finally we simulate room with the correct modal frequencies, $k_n = n\frac{\pi}{L_x}$, while we also include more prior knowledge, as discussed in Section IV. We only simulate the positive frequencies, thus the first $\frac{N-1}{2}$ columns of $\mathbf{A}$ are omitted. We use $M = M_o = M_t = 15$, $L_x = 5$, $F = 3$, the source emits $L = 50$ frequencies, which are i.i.d., $\omega_l \sim \mathcal{U}[0, c\pi F)$. We solve the SDP in (20). The magnitude of the dual polynomial of the problem is shown in Fig. 5, which attains one exactly at the modal frequencies. The RMSE of the estimated frequencies is in the order of 10^{-8}. The total CPU time for the SDP in (20) is 9.33 seconds on an Intel Core i7-6700HQ.

VI. CONCLUSION

We have investigated if we can estimate the room modes using the atomic norm, a gridless method. We have derived a bound for the sound field reconstruction problem and relate this to the frequency separation that is required by the atomic norm for perfect reconstruction. We show that prior knowledge has to be included to be able to reach perfect reconstruction by the atomic norm. We describe two strategies that, in conjunction, can be used to realize successful recovery. Our findings are confirmed by numerical simulations.

REFERENCES

[1] S. Cecchi, A. Carini, and S. Spors, “Room response equalization — A review,” *Appl. Sci.*, vol. 8, no. 1, 2018, Art. no. 16.

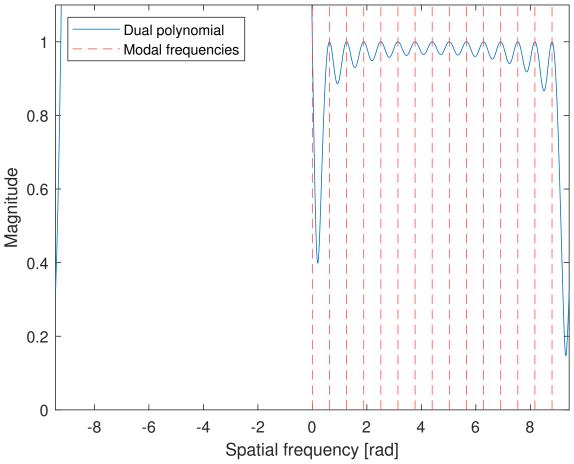

Fig. 5. Magnitude of dual polynomial, $M = 15, L = 50$

[2] P. A. Naylor and N. D. Gaubitch, *Speech Dereverberation*. New York, NY, USA: Springer, 2010.

[3] T. Betlehem, W. Zhang, M. A. Poletti and T. D. Abhayapala, ”Personal Sound Zones: Delivering interface-free audio to multiple listeners,” in *IEEE Signal Process. Mag.*, vol. 32, no. 2, pp. 81-91, March 2015.

[4] F. Lluís, P. Martínez-Nuevo, M. Møller and S. E. Shepstone, ”Sound field reconstruction in rooms: inpainting meets super-resolution,” *J. Acoust. Soc. Am.*, vol. 148, no. 2, pp. 649–659, 2020.

[5] T. P. Vu and H. Lissek, ”Low frequency sound field reconstruction in a non-rectangular room using a small number of microphones,” *Acta Acust.*, vol. 4, no. 2, 2020.

[6] S. A. Verburg, and E. F. Grande, ”Reconstruction of the sound field in a room using compressive sensing,” *J. Acoust. Soc. Am.*, vol. 143, no. 6, pp. 3770–3779, 2018.

[7] E. F. Grande, “Sound field reconstruction in a room from spatially distributed measurements,” in *Proc. 23rd Int. Congr. on Acoust.*, 2019, pp. 4961–4968.

[8] R. Tibshirani, ”Regression Shrinkage and Selection via the Lasso,” *J. Roy. Stat. Soc. Ser. B*, vol. 58, no. 1, 1996, pp. 267–288.

[9] Y. Chi, L. L. Scharf, A. Pezeshki and A. R. Calderbank, ”Sensitivity to Basis Mismatch in Compressed Sensing,” *IEEE Trans. Signal Process.*, vol. 59, no. 5, pp. 2182-2195, May 2011.

[10] Y. Chi, ”Joint sparsity recovery for spectral compressed sensing,” in *Proc. 2014 IEEE Int. Conf. Acoust., Speech, Signal Process. (ICASSP)*, 2014, pp. 3938-3942.

[11] E. Candès and C. Fernandez-Granda, ”Towards a Mathematical Theory of Super-Resolution,” in *Commun. Pure Appl. Math.*, vol. 67, no.6, pp. 906–956, 2014.

[12] G. Tang, B. N. Bhaskar, P. Shah and B. Recht, ”Compressed Sensing Off the Grid,” *IEEE Trans. Inform. Theory*, vol. 59, no. 11, pp. 7465-7490, Nov. 2013.

[13] H. Kuttruff, ”The sound field in a closed space,” in *Room acoustics*, 4th ed. London: Spon Press, 2005.

[14] E. J. Candes and M. B. Wakin, ”An Introduction To Compressive Sampling,” in *IEEE Signal Process. Mag.*, vol. 25, no. 2, pp. 21-30, March 2008.

[15] Z. Yang and L. Xie, ”Exact Joint Sparse Frequency Recovery via Optimization Methods,” *IEEE Trans. Signal Process.*, vol. 64, no. 19, pp. 5145-5157, Oct. 2016.

[16] T. Ajdler, L. Sbaiz and M. Vetterli, ”Dynamic measurement of room impulse responses using a moving microphone,” *J. Acoust. Soc. Am.*, vol. 122, no. 3, pp. 1636–1645, 2007.

[17] H. Chao and L. Vandenberghe, ”Extensions of semidefinite programming methods for atomic decomposition,” in *Proc. 2016 IEEE Int. Conf. Acoust., Speech, Signal Process. (ICASSP)*, 2016, pp. 4757-4761.

[18] R. Roy and T. Kailath, ”ESPRIT-estimation of signal parameters via rotational invariance techniques,” *IEEE Trans. Acoust., Speech, Signal Process.*, vol. 37, no. 7, pp. 984-995, Jul. 1989.

B

Derivation of the Sound Field Expression for a 1D Room with Rigid Walls

In this appendix we show the derivation of the sound field in a one-dimensional room with rigid walls.

Derivation

We begin with the homogeneous wave equation

$$\frac{\partial^2 u}{\partial x^2} - \frac{1}{c^2}\frac{\partial^2 u}{\partial t^2} = 0 \tag{B.1}$$

where c is the wave speed in the medium. We suppose that the solution can be separated with respect to the variables.

$$u(x,t) = u(x)u(t) \tag{B.2}$$

We then first look at the Helmholtz equation, which the part $u(x)$ needs to satisfy

$$\frac{\partial^2 u(x)}{\partial x^2} + k^2 u(x) = 0, \quad k = \frac{\omega}{c} \tag{B.3}$$

where ω is the temporal (angular) frequency. We try the following solution,

$$u(x) = Ae^{jk_x x} + Be^{-jk_x x} \tag{B.4}$$

and fill it into the Helmholtz equation to get

$$\begin{aligned} -Ak_x^2 e^{jk_x x} - Bk_x^2 e^{-jk_x x} + k^2 u(x) &= 0 \\ u(x)(k^2 - k_x^2) &= 0 \\ k_x^2 &= k^2. \end{aligned} \tag{B.5}$$

Now, since we are looking for a solution in a 1D room with rigid walls at $x = 0$ and $x = L_x$, we have two boundary conditions, of which the first leads to

$$\begin{aligned}
\left.\frac{\partial u(x)}{\partial x}\right|_{x=0} &= 0 \\
\left.(Ajke^{jkx} + -Bjke^{-jkx})\right|_{x=0} &= 0 \\
(Ajk - Bjk) &= 0 \\
A &= B
\end{aligned} \tag{B.6}$$

and the second leads to

$$\begin{aligned}
\left.\frac{\partial u(x)}{\partial x}\right|_{x=L_x} &= 0 \\
\left.(Ajke^{jkx} + -Ajke^{-jkx})\right|_{x=L_x} &= 0 \\
(Ajke^{jkL_x} - Ajke^{-jkL_x}) &= 0 \\
Ajk(e^{jkL_x} - e^{-jkL_x}) &= 0 \\
-2Ak\sin(kL_x) &= 0 \\
k &= \frac{n\pi}{L_x}, \quad n \in \mathbb{Z}.
\end{aligned} \tag{B.7}$$

Thus only discrete values of $k_n = \frac{n\pi}{L_x}$ are allowed in the solution $u(x)$. To form the general solution to the homogeneous Helmholtz equation, eq. (B.3), we consider all of these discrete frequencies

$$u(x) = \sum_{n\in\mathbb{N}} (A_n e^{jk_n x} + A_n e^{-jk_n x}) = \sum_{n\in\mathbb{N}} B_n \cos(k_n x). \tag{B.8}$$

Thus, if there is no source, the sound field can be described by eq. (B.8).

Now we would also like to find a solution to the in-homogeneous Helmholtz equation

$$\frac{\partial^2 u(x)}{\partial x^2} + k^2 u(x) = f(x), \quad k = \frac{\omega}{c}. \tag{B.9}$$

To get the solution to eq. (B.9), we first need to find the so called Green's function G, which is the solution to

$$\frac{\partial^2 G(x, x_0)}{\partial x^2} + k^2 G(x, x_0) = -\delta(x - x_0). \tag{B.10}$$

More over, G, should also satisfy the previously mentioned boundary conditions. We know from the derivations above that the solution G should be of the form of the general solution,

$$G(x, x_0) = \sum_{n\in\mathbb{N}} C_n \cos(k_n x). \tag{B.11}$$

Also, we write the delta function as a combination of cosines,

$$-\delta(x - x_0) = \sum_{n\in\mathbb{N}} D_n \cos(k_n x) \tag{B.12}$$

and try to get an expression for the amplitudes D_n. We multiply both sides of eq. (B.12) by $\cos(k_m x)$, and integrate over the room in space

$$\begin{aligned}\int_0^{L_x}\cos(k_m x)\sum_n D_n\cos(k_n x)dx &= -\int_0^{L_x}\cos(k_m x)\delta(x-x_0)dx\\ D_m\frac{L_x}{2}e^{j\omega_m t} &= -\cos(k_m x_0)\\ D_m &= -\frac{2}{L_x}\cos(k_m x_0).\end{aligned}\tag{B.13}$$

Thus the delta function can be expanded into room modes as follows

$$-\delta(x-x_0)=\sum_{n\in\mathbb{N}}-\frac{2}{L_x}\cos(k_n x_0)\cos(k_n x).\tag{B.14}$$

We now return to finding the coefficients C_n, by filling in the room mode expansions in eq. (B.10) to get

$$\begin{aligned}(\partial_{xx}+k^2)G(x,x_0,t,t_0) &= -\delta(x-x_0)\\ (\partial_{xx}+k^2)\sum_{n\in\mathbb{N}}C_n\cos(k_n x) &= \sum_{n\in\mathbb{N}}-\frac{2}{L_x}\cos(k_n x_0)\cos(k_n x)\\ \sum_{n\in\mathbb{N}}C_n(\partial_{xx}+k_n^2-k_n^2+k^2)\cos(k_n x) &= \sum_{n\in\mathbb{N}}-\frac{2}{L_x}\cos(k_n x_0)\cos(k_n x)\\ \sum_{n\in\mathbb{N}}C_n(-k_n^2+k^2)\cos(k_n x) &= \sum_{n\in\mathbb{N}}-\frac{2}{L_x}\cos(k_n x_0)\cos(k_n x)\\ C_n &= -\frac{2}{L_x}\frac{\cos(k_n x_0)}{k^2-k_n^2},\quad \forall n\in\mathbb{N}.\end{aligned}\tag{B.15}$$

Here the coefficients C_n turn out to depend on the frequency, as $k=\frac{\omega}{c}$. We thus have

$$G(x,x_0,\omega)=-\frac{2}{L_x}\sum_{n\in\mathbb{N}}\frac{\cos(k_n x_0)}{(\frac{\omega}{c})^2-k_n^2}\cos(k_n x).\tag{B.16}$$

Now let's assume we are dealing with a single point source, sucht that $f(x)=\delta(x-x_0)$, then if the source has a band limited support $f(t)=\int_{-\omega_c}^{+\omega_c}F(\omega)e^{j\omega t}d\omega$, we can write

$$\begin{aligned}u(x,t) &= \int_{-\omega_c}^{+\omega_c}\int_0^{L_x}G(x,x',\omega)f(x')F(\omega)e^{j\omega t}dx'd\omega\\ &= \int_{-\omega_c}^{+\omega_c}\int_0^{L_x}-\frac{2}{L_x}\sum_{n\in\mathbb{N}}\frac{\cos(k_n x')}{(\frac{\omega}{c})^2-k_n^2}\cos(k_n x)\delta(x-x_0)F(\omega)e^{j\omega t}dx'd\omega\\ &= \int_{-\omega_c}^{+\omega_c}-\frac{2}{L_x}\sum_{n\in\mathbb{N}}\frac{\cos(k_n x_0)}{(\frac{\omega}{c})^2-k_n^2}\cos(k_n x)F(\omega)e^{j\omega t}d\omega\\ &= -\frac{2}{L_x}\sum_{n\in\mathbb{N}}\cos(k_n x_0)\cos(k_n x)\int_{-\omega_c}^{+\omega_c}\frac{1}{(\frac{\omega}{c})^2-k_n^2}F(\omega)e^{j\omega t}d\omega.\end{aligned}\tag{B.17}$$

For the simple case where the source emits a single frequency ω_0 and we still assume that that the source is a point source located inside the room at $x=x_0$, the sound field can be expressed as

$$\begin{aligned}p(x,t) &= -\frac{2}{L_x}\sum_{n\in\mathbb{N}}\cos(k_n x_0)\cos(k_n x)\int_{-\omega_c}^{+\omega_c}\frac{1}{(\frac{\omega}{c})^2-k_n^2}\delta(\omega-\omega_0)e^{j\omega t}d\omega\\ &= -\frac{2}{L_x}e^{j\omega_0 t}\sum_{n\in\mathbb{N}}\frac{\cos(k_n x_0)}{(\frac{\omega_0}{c})^2-k_n^2}\cos(k_n x).\end{aligned}\tag{B.18}$$

Then, if the source emits multiple frequencies at the same time, with possibly different amplitudes, we can simply add the two sound fields together to write

$$\begin{aligned} p(x,t) &= C_1 e^{j\omega_1 t} \sum_{n\in\mathbb{N}} \frac{\cos(k_n x_0)}{(\frac{\omega_1}{c})^2 - k_n^2} \cos(k_n x) + ... + C_L e^{j\omega_L t} \sum_{n\in\mathbb{N}} \frac{\cos(k_n x_0)}{(\frac{\omega_L}{c})^2 - k_n^2} \cos(k_n x) \\ &= \sum_{l}^{L} C_l \Big[\sum_{n\in\mathbb{N}} \frac{\cos(k_n x_0)}{(\frac{\omega_l}{c})^2 - k_n^2} \cos(k_n x) \Big] e^{j\omega_l t} \end{aligned} \tag{B.19}$$

where $C_l \in \mathbb{R}$ is a constant, which allows for excitation frequencies with varying amplitudes.

Orthogonality of the room modes

In the previous section we have shown that the sound field can be written as a summation over cosines. In general, sound fields can be decomposed into its room modes [13]; in the case of rigid walls, the room modes thus have the shape of cosines, that is

$$\psi_n(x) = \sqrt{2}\cos(k_n x). \tag{B.20}$$

One important property of the room modes is that they are mutually orthogonal. We can show that

$$\int_0^{L_x} \psi_n(x)\psi_m(x) = \begin{cases} L_x, & n = m \\ 0, & n \neq m. \end{cases} \tag{B.21}$$

The derivation is as follows,

$$\begin{aligned} \int_0^{L_x} \psi_n(x)\psi_m(x)\mathrm{d}x &= \int_0^{L_x} 2\cos(k_n x)\cos(k_m x)\mathrm{d}x \\ &= \int_0^{L_x} 2\cos(n\frac{\pi}{L_x}x)\cos(m\frac{\pi}{L_x}x)\mathrm{d}x \\ &= \int_0^{L_x} \cos((n-m)\frac{\pi}{L_x}x) + \cos((n+m)\frac{\pi}{L_x}x)\mathrm{d}x \quad (*) \end{aligned} \tag{B.22}$$

Now we consider two cases, namely $n = m$ and $n \neq m$.

Case: $n = m$ If $n = m$ we can write,

$$\begin{aligned} (*) &= \int_0^{L_x} \cos(0 \cdot \frac{\pi}{L_x}x) + \cos(2n\frac{\pi}{L_x}x)\mathrm{d}x \\ &= 1 \cdot L_x + [\frac{L_x}{n2\pi}\sin(n\frac{2\pi}{L_x}x)]_0^{L_x} \\ &= L_x + 0 = L_x. \end{aligned} \tag{B.23}$$

Case: $n \neq m$ If $n \neq m$ we can write,

$$\begin{aligned} (*) &= [\frac{L_x}{(n-m)\pi}\sin((n-m)\frac{\pi}{L_x}x)]_0^{L_x} + [\frac{L_x}{(n+m)\pi}\sin((n+m)\frac{\pi}{L_x}x)]_0^{L_x} \\ &= 0 + 0 = 0. \end{aligned} \tag{B.24}$$

This result is summarized in Eq. (B.21).

C

Room Modes in a Room with Non-Rigid Walls

In this appendix we show the derivation of the room modes in a room with non-rigid walls.

Derivation

We begin by changing the possible solution into,

$$u(x) = Ae^{jk_x x+\phi_x} + Be^{-(jk_x x+\phi_x)}. \tag{C.1}$$

Now, we look for a solution in a 1D room with non-rigid walls at $x = 0$ and $x = L_x$, with wall impedances ζ_{x0} and ζ_{x1}, we have two boundary conditions, of which the first leads to

$$\begin{aligned} \zeta_{x0}\frac{\partial u(x)}{\partial x}\bigg|_{x=0} &= jku(x)\bigg|_{x=0} \\ \zeta_{x0}(Ajk_x e^{\phi_x} + -Bjk_x e^{-\phi_x}) &= jk(Ae^{\phi_x} + Be^{-\phi_x}) \\ (k-\zeta_{x0}k_x)e^{\phi_x}A + (k+\zeta_{x0}k_x)e^{-\phi_x}B &= 0 \end{aligned} \tag{C.2}$$

thus,

$$A = -\frac{(k+\zeta_{x0}k_x)}{(k-\zeta_{x0}k_x)}e^{-2\phi_x}B. \tag{C.3}$$

We then have

$$\begin{aligned} u(x) &= -\frac{(k+\zeta_{x0}k_x)}{(k-\zeta_{x0}k_x)}e^{-2\phi_x}Be^{jk_x x+\phi_x} + Be^{-(jk_x x+\phi_x)} \\ &= B\frac{e^{-\phi_x}}{(k-\zeta_{x0}k_x)}\big[-(k+\zeta_{x0}k_x)e^{jk_x x} + (k-\zeta_{x0}k_x)e^{-jk_x x}\big] \\ &= C\big[-(k+\zeta_{x0}k_x)e^{jk_x x} + (k-\zeta_{x0}k_x)e^{-jk_x x}\big]. \end{aligned} \tag{C.4}$$

From this expression we can see that if $\zeta_{x0}k_x \gg k$, both exponentials are multiplied by roughly the same factor. As a result $u(x)$ will become a hyperbolic cosine (presuming that the k_x turn out to be complex valued).

We will omit the factor C, as in the end we determine a solution up to a scalar factor.

Then the second boundary condition leads to

$$\begin{aligned}
\zeta_{x1}\frac{\partial u(x)}{\partial x}\bigg|_{x=L_x} &= -jku(x)\bigg|_{x=L_x}\\
\zeta_{x1}\big[-jk_x(k+\zeta_{x0}k_x)e^{jk_xL_x} - jk_x(k-\zeta_{x0}k_x)e^{-jk_xL_x}\big] &= \\
&\quad -jk\big[-(k+\zeta_{x0}k_x)e^{jk_xL_x} + (k-\zeta_{x0}k_x)e^{-jk_xL_x}\big]\\
-\zeta_{x1}k_x(k+\zeta_{x0}k_x)e^{jk_xL_x} - \zeta_{x1}k_x(k-\zeta_{x0}k_x)e^{-jk_xL_x} &= \\
&\quad k(k+\zeta_{x0}k_x)e^{jk_xL_x} - k(k-\zeta_{x0}k_x)e^{-jk_xL_x}\\
-\zeta_{x1}k_x(k+\zeta_{x0}k_x)e^{2jk_xL_x} - \zeta_{x1}k_x(k-\zeta_{x0}k_x) &= k(k+\zeta_{x0}k_x)e^{2jk_xL_x} - k(k-\zeta_{x0}k_x)\\
(k+\zeta_{x1}k_x)(k+\zeta_{x0}k_x)e^{2jk_xL_x} &= (k-\zeta_{x1}k_x)(k-\zeta_{x0}k_x)\\
e^{2jk_xL_x} &= \frac{(k-\zeta_{x1}k_x)(k-\zeta_{x0}k_x)}{(k+\zeta_{x1}k_x)(k+\zeta_{x0}k_x)}
\end{aligned} \tag{C.5}$$

The values of k_x are found by solving the resulting equation in eq. (C.5). However, this equation is nonlinear and finding a closed form solution is still an open problem. Therefore current literature tries to find the roots by means of iterative algorithms, e.g. [38]. Somewhat older literature assume that the room modes will be of the form of hyperbolic cosines [39],

$$\psi(x) = \cosh(jk_xx + \phi_x). \tag{C.6}$$

Consequently, the first boundary condition results in

$$\begin{aligned}
\zeta_{x0}\frac{\partial \psi(x)}{\partial x}\bigg|_{x=0} &= jk\psi(x)\bigg|_{x=0}\\
\zeta_{x0}jk_x\sinh(jk_xx+\phi_x)\bigg|_{x=0} &= jk\cosh(jk_xx+\phi_x)\bigg|_{x=0}\\
\coth(\phi_x) &= \frac{\zeta_{x0}k_x}{k}\\
\phi_x &= \coth^{-1}(\frac{\zeta_{x0}k_x}{k}).
\end{aligned} \tag{C.7}$$

Then the second boundary condition results in

$$\begin{aligned}
\zeta_{x1}\frac{\partial \psi(x)}{\partial x}\bigg|_{x=L_x} &= -jk\psi(x)\bigg|_{x=L_x}\\
\zeta_{x1}jk_x\sinh(jk_xx+\phi_x)\bigg|_{x=L_x} &= -jk\cosh(jk_xx+\phi_x)\bigg|_{x=L_x}\\
\coth(jk_xL_x+\phi_x) &= -\frac{\zeta_{x1}k_x}{k}\\
jk_xL_x+\phi_x &= \coth^{-1}(-\frac{\zeta_{x1}k_x}{k}).
\end{aligned} \tag{C.8}$$

And thus, combining eq. (C.7) and eq. (C.8), the k_x can be found by solving eq. (C.9). Bistafa *et al.* presented a numerical procedure of solving eq. (C.9)[40].

$$jk_xL_x + \coth^{-1}(\frac{\zeta_{x0}k_x}{k}) + \coth^{-1}(\frac{\zeta_{x1}k_x}{k}) = 0 \tag{C.9}$$

D

Proof of Theorem 2.2.3

In this appendix we give the proof Theorem 2.2.3.

Theorem 2.2.3

We begin by restating the theorem.

Theorem. *Suppose* $\mathbf{U} = \begin{bmatrix} \mathbf{A} & \mathbf{B}^H \\ \mathbf{B} & \mathbf{C} \end{bmatrix} \in \mathbb{C}^{N\times N}$*. Then,* $\mathbf{U} \succcurlyeq 0$ *if and only if* $\begin{bmatrix} \mathbf{C} & \mathbf{B} \\ \mathbf{B}^H & \mathbf{A} \end{bmatrix} \succcurlyeq 0$.

Proof

The proof of the above theorem is as follows.

Proof.

$$
\begin{aligned}
& \begin{bmatrix} \mathbf{A} & \mathbf{B}^H \\ \mathbf{B} & \mathbf{C} \end{bmatrix} \succcurlyeq 0 \\
\iff & [x_1^H x_2^H] \begin{bmatrix} \mathbf{A} & \mathbf{B}^H \\ \mathbf{B} & \mathbf{C} \end{bmatrix} \begin{bmatrix} \mathbf{x}_1 \\ \mathbf{x}_2 \end{bmatrix} \geq 0, \quad \begin{bmatrix} \mathbf{x}_1 \\ \mathbf{x}_2 \end{bmatrix} \in \mathbb{C}^N \\
\iff & \mathbf{x}_1^H \mathbf{A} \mathbf{x}_1 + \mathbf{x}_1^H \mathbf{B}^H \mathbf{x}_2 + \mathbf{x}_2^H \mathbf{B} \mathbf{x}_1 + \mathbf{x}_2^H \mathbf{C} \mathbf{x}_2 \geq 0 \\
\iff & (\mathbf{x}_1^H \mathbf{A} \mathbf{x}_1 + \mathbf{x}_1^H \mathbf{B}^H \mathbf{x}_2 + \mathbf{x}_2^H \mathbf{B} \mathbf{x}_1 + \mathbf{x}_2^H \mathbf{C} \mathbf{x}_2)^H \geq 0 \\
\iff & \mathbf{x}_1^H \mathbf{A}^H \mathbf{x}_1 + \mathbf{x}_1^H \mathbf{B} \mathbf{x}_2 + \mathbf{x}_2^H \mathbf{B}^H \mathbf{x}_1 + \mathbf{x}_2^H \mathbf{C}^H \mathbf{x}_2 \geq 0 \\
\iff & [\mathbf{x}_2^H \mathbf{x}_1^H] \begin{bmatrix} \mathbf{C}^H & \mathbf{B}^H \\ \mathbf{B} & \mathbf{A}^H \end{bmatrix} \begin{bmatrix} \mathbf{x}_2 \\ \mathbf{x}_1 \end{bmatrix} \geq 0, \quad \begin{bmatrix} \mathbf{x}_2 \\ \mathbf{x}_1 \end{bmatrix} \in \mathbb{C}^N \\
\iff & \begin{bmatrix} \mathbf{C}^H & \mathbf{B}^H \\ \mathbf{B} & \mathbf{A}^H \end{bmatrix} \succcurlyeq 0 \\
\iff & \begin{bmatrix} \mathbf{C} & \mathbf{B} \\ \mathbf{B}^H & \mathbf{A} \end{bmatrix} \succcurlyeq 0
\end{aligned}
\tag{D.1}
$$

□